Arne P. Willner | Sandra M. Barr | Johannes Glodny
Hans-Joachim Massonne | Masafumi Sudo
Stuart N. Thomson | Cees R. Van Staal | Chris E. White

Effects of fluid flow, cooling and deformation as recorded by 40Ar/39Ar, Rb–Sr and zircon fission track ages in very low- to low-grade metamorphic rocks in Avalonian SE Cape Breton Island

Suggested citation referring to the original publication:
Geological Magazine 152 (2015) 5, pp. 767–787
DOI https://doi.org/10.1017/S0016756814000508
ISSN (print) 0016-7568
ISSN (online) 1469-5081

Geol. Mag. **152** (5), 2015, pp. 767–787. © Cambridge University Press 2014
doi:10.1017/S0016756814000508

Effects of fluid flow, cooling and deformation as recorded by $^{40}Ar/^{39}Ar$, Rb–Sr and zircon fission track ages in very low- to low-grade metamorphic rocks in Avalonian SE Cape Breton Island (Nova Scotia, Canada)

ARNE P. WILLNER*†‡, SANDRA M. BARR§, JOHANNES GLODNY¶, HANS-JOACHIM MASSONNE*, MASAFUMI SUDO‖, STUART N. THOMSON#, CEES R. VAN STAAL** & CHRIS E. WHITE††

*Institut für Mineralogie und Kristallchemie, Universität Stuttgart, Azenbergstr. 18, 70174 Stuttgart, Germany
‡Institut für Geologie, Mineralogie und Geophysik, Ruhr-Universität, 44780 Bochum, Germany
§Department of Earth and Environmental Science, Acadia University, Wolfville, Nova Scotia B4P 2R6, Canada
¶Deutsches GeoForschungsZentrum GFZ, Telegrafenberg, D-14473 Potsdam, Germany
‖Institut für Erd- und Umweltwissenschaften, Universität Potsdam, Karl-Liebknecht-Str. 24, D-14476 Potsdam-Golm, Germany
#Department of Geosciences, University of Arizona, 1040 E. 4th St, Tucson, AZ 85721-0077, USA
**Geological Survey of Canada, 625 Robson Street, Vancouver, BC V6B 5J3, Canada
††Nova Scotia Department of Natural Resources, PO Box 698, Halifax, Nova Scotia B3J 2T9, Canada

(*Received* 13 May 2014; *accepted* 15 August 2014; *first published online* 11 November 2014)

Abstract – $^{40}Ar/^{39}Ar$ *in situ* UV laser ablation of white mica, Rb–Sr mineral isochrons and zircon fission track dating were applied to determine ages of very low- to low-grade metamorphic processes at 3.5 ± 0.4 kbar, 280 ± 30 °C in the Avalonian Mira terrane of SE Cape Breton Island (Nova Scotia). The Mira terrane comprises Neoproterozoic volcanic-arc rocks overlain by Cambrian sedimentary rocks. Crystallization of metamorphic white mica was dated in six metavolcanic samples by $^{40}Ar/^{39}Ar$ spot age peaks between 396 ± 3 and 363 ± 14 Ma. Rb–Sr systematics of minerals and mineral aggregates yielded two isochrons at 389 ± 7 Ma and 365 ± 8 Ma, corroborating equilibrium conditions during very low- to low-grade metamorphism. The dated white mica is oriented parallel to foliations produced by sinistral strike-slip faulting and/or folding related to the Middle–Late Devonian transpressive assembly of Avalonian terranes during convergence and emplacement of the neighbouring Meguma terrane. Exhumation occurred earlier in the NW Mira terrane than in the SE. Transpression was related to the closure of the Rheic Ocean between Gondwana and Laurussia by NW-directed convergence. The $^{40}Ar/^{39}Ar$ spot age spectra also display relict age peaks at 477–465 Ma, 439 Ma and 420–428 Ma attributed to deformation and fluid access, possibly related to the collision of Avalonia with composite Laurentia or to earlier Ordovician–Silurian rifting. Fission track ages of zircon from Mira terrane samples range between 242 ± 18 and 225 ± 21 Ma and reflect late Palaeozoic reburial and reheating close to previous peak metamorphic temperatures under fluid-absent conditions during rifting prior to opening of the Central Atlantic Ocean.

Keywords: $^{40}Ar/^{39}Ar$ spot ages, Rb–Sr mineral isochrons, zircon fission tracks, very low-/low-grade metamorphism, Avalonia, Devonian transpression, Rheic Ocean.

1. Introduction

Knowledge of the timing of metamorphic processes in combination with pressure and temperature estimates from local mineral equilibria preserved in metamorphic rocks is indispensable for the reconstruction and quantification of geological processes along pressure–temperature–time paths and the understanding of tectonics in three dimensions. Few studies of this type have been conducted in areas with very low- to low-grade (subgreenschist to greenschist facies) metamorphic overprint compared to higher grade regions, because the metamorphic overprint is less obvious compared to primary features. Furthermore, studies of very low- and low-grade metamorphism are generally hampered by small grain size, strong chemical variation and the prevailing idea of 'disequilibrium'. Here we present the results of a geochronological study that follows up on a detailed petrological investigation of metamorphic processes at very low- to low-grade conditions in the Avalonian Mira terrane of SE Cape Breton Island (Willner *et al.* 2013*b*).

Isotopic systems available for dating metamorphism at very low- and low-grade conditions are relatively limited, and the systems date very different processes. For dating white mica, the $^{40}Ar/^{39}Ar$ and Rb–Sr systems are the most suitable. Peak metamorphic temperatures

†Author for correspondence: arne.willner@rub.de

in the study area of 280 ± 30 °C in the Mira terrane (Willner *et al.* 2013*b*) are well below the frequently cited range of white mica Ar closure temperatures of *c.* 350–420 °C (McDougall & Harrison, 1999), although it was argued by Villa (1998, 2006) that strain and fluid availability are more important in isotope redistribution for the $^{40}Ar/^{39}Ar$ system and hence that many estimates of its closure temperature are too low. This point was also made by Wijbrans & McDougall (1986), who suggested that closure by volume diffusion will only occur in the absence of other faster processes such as strain-induced recrystallization. Crystallization of white mica is dated with the $^{40}Ar/^{39}Ar$ system at very low and low metamorphic grades, but two processes can also lead to recystallization and resetting of ages at low metamorphic temperatures: deformation (e.g. Müller *et al.* 1999), fluid access inducing mineral reactions or dissolution-reprecipitation processes (e.g. Willner *et al.* 2009, 2012), or a combination of both. These processes can induce age heterogeneity at thin-section and outcrop scale and, if recrystallization or dissolution-reprecipitation of mica is incomplete, also mixing of ages. To detect such potential heterogeneities in the study area, we applied $^{40}Ar/^{39}Ar$ spot age dating using UV laser ablation techniques (Kelley, Arnaud & Turner, 1994).

Rb–Sr internal mineral isochron data are particularly suitable to directly date mineral reactions and hence metamorphic equilibrium assemblages, but also ductile deformation in white mica-bearing rocks. Deformation-induced recrystallization of white mica and associated phases will generally lead to complete Sr-isotopic re-equilibration and resetting of ages (Inger & Cliff, 1994; Müller *et al.* 1999). Such resetting of ages dates the last recrystallization-inducing process, that is, the waning stages of deformation (Freeman *et al.* 1998), providing that no later thermal-diffusive or retrogressive overprint occurred. Diffusional resetting of the Rb–Sr system in white mica is activated only at amphibolite-facies temperatures of >550 °C (cf. Villa, 1998). In the set of samples used in this study (the properties of which are listed in Table 1), peak metamorphic temperatures were generally lower so that post-crystallization Rb and Sr diffusion processes can likely be ruled out.

Fission tracks in zircon shorten or anneal with increased temperature and duration of heating. For pristine zircon grains, annealing over geological time begins at 250 ± 20 °C with total resetting occurring above 310 ± 20 °C (Tagami *et al.* 1998), although these temperatures are lower in zircon with high accumulated radiation damage (Rahn *et al.* 2004). The typical closure temperature of 280 ± 30 °C for fission tracks in zircon at commonly realized moderate-to-fast cooling rates correlates well with the brittle/ductile transition (Brix *et al.* 2002), and is somewhat lower than peak metamorphic temperatures estimated in the study area (Willner *et al.* 2013).

In this paper we apply all three of these dating methods to very low- to low-grade metavolcanic and metasedimentary rocks of the Mira terrane (Willner *et al.* 2013*b*). Our purpose is to determine where complete isotopic homogenization occurred and where it did not, in order to understand which processes are being dated and which control microchemical and isotopic homogenization. We also aim to derive a history of these processes, contributing to the refinement of current tectonic models.

2. Geological setting and previously published age data

The very low- to low-grade metamorphic rocks of the Mira terrane in SE Cape Breton Island (Barr & Raeside, 1989) are part of the West Avalonian microplate (Fig. 1). As in other parts of West Avalonia, the Mira terrane is characterized by late Neoproterozoic metavolcanic, metasedimentary and plutonic rocks unconformably overlain by Cambrian sedimentary strata. The terrane consists of five juxtaposed volcanic-sedimentary-plutonic belts with differences in their late Neoproterozoic – early Cambrian history: (1) Stirling; (2) East Bay Hills; (3) Coxheath Hills; (4) Sporting Mountain; and (5) Coastal. These belts are interpreted as originally separate parts of an extended magmatic arc system (Barr, 1993; Barr, White & Macdonald, 1996).

The Stirling belt comprises metasedimentary and metavolcanic rocks (Stirling Group) with protolith ages (U–Pb zircon) of 681–620 Ma (Bevier *et al.* 1993; Willner *et al.* 2013*a*) intruded by granodiorite at 620 + 3/– 2 Ma (U–Pb zircon; Barr *et al.* 1990). The protoliths of the Stirling Group were predominantly andesitic to basaltic lapilli tuff and epiclastic turbiditic deposits (litharenite, siltstone) with subordinate basaltic flows and breccias, rhyolitic lapilli tuff and rhyolite porphyry, intruded by comagmatic gabbroic dykes and sills and including a massive sulphide deposit (Macdonald & Barr, 1993*a*; Barr, White & Macdonald, 1996). The Stirling Group likely formed within a calc-alkaline volcanic arc but under marine conditions (Macdonald & Barr, 1993*a*; Barr, White & Macdonald, 1996).

The East Bay Hills, Coxheath Hills and Sporting Mountain belts consist mainly of subaerial metavolcanic and metavolcaniclastic rocks of basaltic, andesitic and rhyolitic composition (East Bay Hills, Coxheath and Pringle Mountain groups) with protolith ages of 623–575 Ma (U–Pb zircon; Bevier *et al.* 1993; Barr, White & Macdonald, 1996; White, Barr & Ketchum, 2003; Willner *et al.* 2013*a*) intruded by *c.* 620 Ma dioritic to granitic plutons (Barr *et al.* 1990; Bevier *et al.* 1993). The three belts are considered to represent a single continental margin volcanic-arc complex (Barr, White & Macdonald, 1996).

In the Coastal belt, two major metavolcanic-metasedimentary units are distinguished (Barr, White & Macdonald, 1996). The Fourchu Group dominantly consists of dacitic lapilli and ash tuff as well as subordinate lava flows and basaltic, andesitic and rhyolitic tuff. A dacitic tuff and comagmatic granitic pluton yielded igneous crystallization ages (U–Pb, zircon) of

https://doi.org/10.1017/S0016756814000508

Table 1. Characteristics of analysed samples (sf – strongly foliated; mf – moderately foliated; wf – weakly foliated; nf – non-foliated)

Sample	Latitude N	Longitude W	Rock type	$^{40}Ar/^{39}Ar$ age (Ma)	Rb–Sr age (Ma)	Zircon FT age (Ma)	Stratigraphic unit	Deformation
10Ca11	45° 43′ 17.5″	60° 20′ 31.3″	Felsic metavolcanic rock	388 ± 18			Fourchu Group	wf
10Ca18	45° 58′ 41.1″	60° 14′ 48.8″	Quartzite			227 ± 18	Sgadan Lake Formation	nf
10Ca29	45° 44′ 37.5″	60° 23′ 14.2″	Volcanogenic metasandstone			232 ± 52	Kelvin Glen Group	nf
10Ca34	45° 43′ 23.9″	60° 21′ 30.5″	Felsic metavolcanic rock	363 ± 7			Fourchu Group	sf
10Ca36	45° 37′ 30.9″	60° 41′ 23.5″	Volcanogenic metasandstone				Stirling Group	nf
10Ca37	45° 54′ 06.7″	60° 30′ 24.7″	Felsic metavolcanic rock	393 ± 2		242 ± 18	East Bay Hills Group	sf
10Ca40	45° 49′ 25.0″	60° 40′ 12.9″	Volcanoclastic metasediment			151 ± 19	East Bay Hills Group	sf
10Ca42	45° 48′ 52.4″	60° 40′ 57.7″	Felsic metavolcanic rock	385 ± 2			East Bay Hills Group	sf
10Ca43	45° 34′ 39.4″	60° 42′ 41.7″	Granite boulder in conglomerate			225 ± 21	Coxheath Group	nf
11Ca05	45° 43′ 24.4″	60° 21′ 30.2″	Mafic metavolcanic rock		365 ± 8		Fourchu Group	wf
11Ca13	45° 51′ 07.4″	60° 38′ 03.4″	Felsic metavolcanic rock		389 ± 7		East Bay Hills Group	sf
11Ca15	45° 41′ 55.3″	61° 03′ 43.9″	Felsic volcanoclastic metasediment	396 ± 2, 420 ± 1, 477 ± 3			Pringle Mountain Group	mf
11Ca18	45° 42′ 02.3″	61° 04′ 02.2″	Felsic volcanoclastic metasediment	439 ± 2, 465 ± 3, 525 ± 5			Pringle Mountain Group	wf

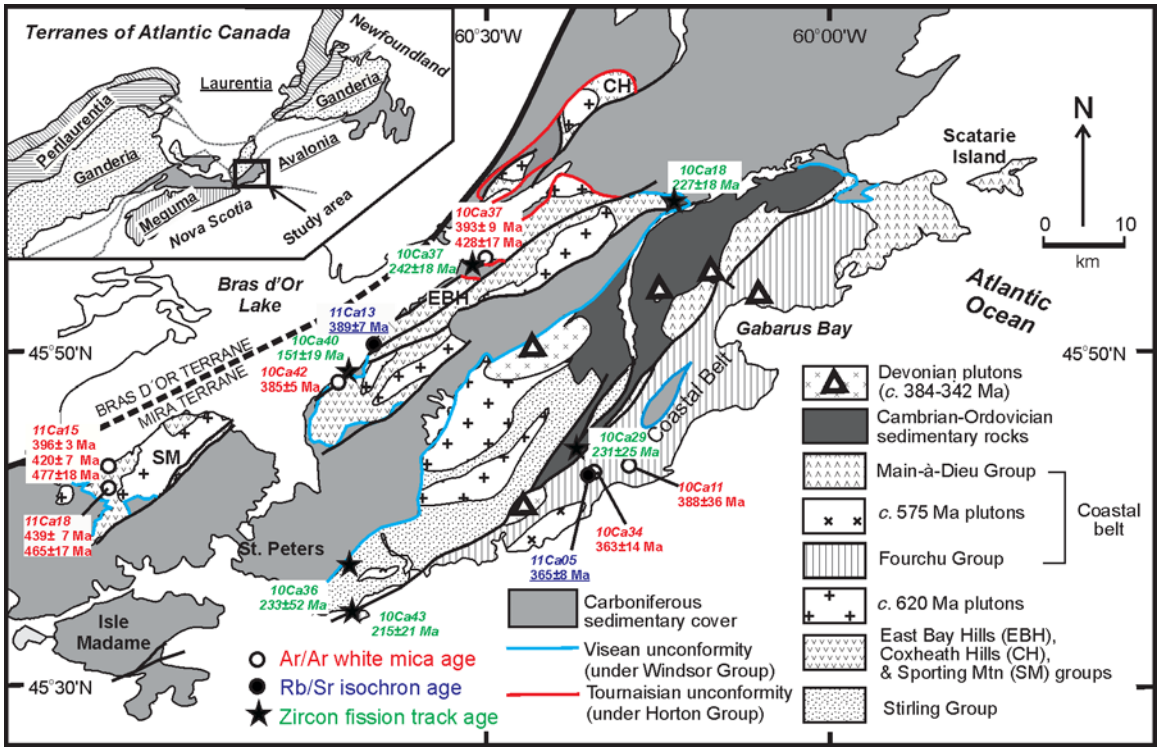

Figure 1. Simplified geological map of southeastern Cape Breton Island after Barr *et al.* (1996), Giles *et al.* (2010) and McMullin *et al.* (2010). The inset map shows the location of the Mira terrane within Avalonia and the terrane assemblage of the northern Appalachian orogen after Hibbard *et al.* (2006). Sample locations and derived ages are indicated.

574 ± 1 Ma and 574 ± 3 Ma (Bevier *et al.* 1993). In contrast, the Main-à-Dieu Group mainly comprises bimodal tuffaceous sedimentary and epiclastic rocks with subordinate basaltic and rhyolitic flows and tuff. A maximum age of *c.* 563 Ma was reported by Bevier *et al.* (1993) based on U–Pb (zircon) dating of a rhyolite flow, and the minimum age is constrained by overlying lower Cambrian sedimentary rocks (Hutchinson, 1952; Landing, 1991; Barr, White & Macdonald, 1996). The Fourchu Group is interpreted to have formed by calc-alkaline volcanism in a continental margin arc and the Main-à-Dieu Group during related intra-arc extension.

https://doi.org/10.1017/S0016756814000508

Barr, White & Macdonald (1996) and Willner *et al.* (2013*a*) proposed that the Stirling, East Bay Hills, Coxheath Hills, Sporting Mountain and Coastal belts represent parts of Neoproterozoic continental magmatic arcs which were active during the period 680–550 Ma at the margin of the likely source continent Amazonia, from which they separated to form part of the Avalonia microcontinent.

Upper Ediacaran – lower Cambrian clastic sedimentary rocks overlie the older rocks, slightly disconformably in the case of the older units but perhaps conformably in the case of the Main-à-Dieu Group (Barr, White & Macdonald, 1996). The Neoproterozoic–Cambrian sedimentary rocks do not form a single stratigraphic succession and have been assigned different (informal) formation names in different areas (Barr, White & Macdonald, 1996). The Kelvin Glen Group (arkose, conglomerate and siltstone) occurs in the Stirling belt, whereas the Bengal Road formation (conglomerate, quartzite and siltstone) and overlying Sgadan Lake formation (quartz sandstone and conglomerate) are situated mainly in the Coastal belt and in a small area at the NE tip of the East Bay Hills belt. In all three areas, these older units are overlain by a succession of fossiliferous finer grained clastic and minor carbonate rocks of early Cambrian – Early Ordovician age (Hutchinson, 1952; Landing, 1991; Palacios *et al.* 2009). Sandstone of the Bengal Road formation contains detrital white mica with $^{40}Ar/^{39}Ar$ ages ranging from 634 to 469 Ma, but dominantly >550 Ma (Reynolds, Barr & White, 2009).

Potter, Longstaffe & Barr (2008) and Potter *et al.* (2008) detected a pervasive low-$\delta^{18}O$ anomaly in Neoproterozoic igneous rocks of the Mira terrane and also in other parts of Avalonia. They interpreted this depletion event as due to an influx of large volumes of post-magmatic meteoric fluids during late Neoproterozoic – early Cambrian trans-tension causing pervasive hydrothermal alteration. Barr, White & Macdonald (1996) and Willner *et al.* (2013*a*) proposed that the Stirling, East Bay Hills, Coxheath Hills, Sporting Mountain and Coastal belts were mostly juxtaposed by brittle strike-slip processes during middle Cambrian time. Rift basins developed, in which sediments were deposited on the structurally amalgamated belts. The pervasive hydrothermal alteration might also have continued during these processes.

Both the Neoproterozoic volcanic-sedimentary-plutonic belts and the upper Ediacaran – lower Ordovician sedimentary cover rocks were overprinted by very low- to low-grade regional metamorphism and mainly ductile deformation. McMullin, Barr & Raeside (2010) deduced regional metamorphic conditions transitional between the prehnite-actinolite facies and greenschist facies in the Neoproterozoic volcanic and sedimentary units. In the vicinity of Devonian plutons, amphibolite facies was attained as a result of contact metamorphism (Macdonald & Barr, 1993*b*; McMullin, Barr & Raeside, 2010). Willner *et al.* (2013*b*) estimated metamorphic conditions in the range of 3.5 ± 0.4 kbar and 280 ± 30 °C in all of the volcanic-sedimentary belts and, in contrast to McMullin, Barr & Raeside (2010), ascribed regional metamorphism to the collisional assembly of West Avalonia during Devonian time rather than solely to non-orogenic burial.

3. Structural geology and age constraints of deformation and accretion

The Stirling Group is characterized by pronounced NE–SW-trending upright to northwesterly overturned folds of variable scale (centimetre- to kilometre-scale; D_1), generally with a moderate plunge to the NE (Macdonald & Barr, 1993*a*; Barr, White & Macdonald, 1996). These folds vary in intensity and scale, likely due to competency contrasts between the strongly variable lithologies and the heterogeneous nature of the deformation. Widely spaced axial planar cleavage (S_1) defined by white mica and chlorite is associated with the F_1 folding in the Stirling Group; deformation is polyphase and possibly of different ages (Macdonald & Barr, 1993*a*). In the SE part of the belt in particular, more strongly foliated shear zones (D_2) up to a few metres in width are locally superimposed on the S_1 foliation (Macdonald & Barr, 1993*a*; Barr, White & Macdonald, 1996).

In contrast to the Stirling Group, the East Bay Hills, Pringle Mountain, Coxheath and Fourchu groups generally lack evidence of F_1 folds and have been overprinted and dissected by prominent steep NE-trending shear zones (D_2). These zones have a thickness of hundreds of metres and are characterized by a well-developed continuous steep NW- or SE-dipping foliation (S_2). They are also characterized by conspicuous strain gradients at the metre-scale from undeformed to mylonitic and are locally associated with steeply plunging chevron folds and kink bands, which fold S_2. Shear-sense indicators suggest that the shear zones mainly accommodated sinistral transcurrent movements. However, some of the major D_2 shear zones are markedly curviplanar such that they form restraining bends (Barr, White & Macdonald, 1996), suggesting that they may have these fault zones may have accommodated a more complex movement history than solely strike-slip. The latter is consistent with the metamorphic evidence for significant tectonic burial (Willner *et al.* 2013*b*).

In contrast to the Fourchu and older groups described above, the Main-à-Dieu Group and overlying Cambrian cover rocks show open folds broadly concordant with the folds in the Stirling Group. Slaty cleavage is developed only locally in fine-grained rocks, although recrystallization of quartz in the matrix of the clastic fabric in some coarser grained samples suggests a similar metamorphic overprint as in the underlying volcanic and sedimentary rocks (Willner *et al.* 2013*b*). Hence, both folding and regional low- to very low-grade metamorphism are considered to have occurred during post-Cambrian time. High-level Devonian plutons intruded locally at $378 + 5/-1$ Ma (Lower St Esprit Pluton, U–Pb zircon; Bevier *et al.* 1993) and 371 ± 1.7 Ma (Gillis

https://doi.org/10.1017/S0016756814000508

Mountain Pluton, U–Pb zircon; unpublished data), although a wider range of 384–342 Ma is indicated by older Rb–Sr and K–Ar dates (Barr & Macdonald, 1992; Macdonald & Barr, 1993*b*). Based on their petrological similarities, all of these plutons are likely to have been comagmatic at *c.* 378–370 Ma (Barr & Macdonald, 1992). The plutons have I-type to A-type chemical affinities and are associated with porphyry and skarn-type mineralization; they produced cordierite-bearing contact metamorphic aureoles, which overprinted the regional very low- to low-grade metamorphism and associated structures. They are generally unfoliated, but locally display D_2 cataclasis and/or mylonitization (Barr & Macdonald, 1992). D_1 therefore predated, and D_2 partly overlapped with, intrusion of the Late Devonian plutons, assuming that all of the shear zones ascribed to D_2 represent a single, likely protracted, event.

The minimum age of juxtaposition of the Avalonian Mira terrane and the now-adjacent Bras d'Or terrane, considered to be part of Ganderia (Raeside & Barr, 1990; Hibbard *et al.* 2006), is constrained by the presence of clasts derived from both Mira and Bras d'Or terranes in conglomerate of the Middle Devonian McAdams Lake Formation NW of the Coxheath Hills belt (White & Barr, 1998). Movement on faults continued at least locally well into Carboniferous time (Gibling *et al.* 2008). Clastic sedimentary rocks and lower Carboniferous (Tournaisian–Visean) limestone of the Horton and Windsor groups unconformably overlie the older rocks of the Mira terrane (Martel & Gibling, 1995; Boehner, Adams & Giles, 2002).

4. Analytical methods

4.a. $^{40}Ar/^{39}Ar$ geochronology

$^{40}Ar/^{39}Ar$ dating was performed in the $^{40}Ar/^{39}Ar$ geochronology laboratory at Universität Potsdam/Germany after neutron activation on six polished rock sections (8 mm diameter) at the nuclear reactor of NRG (Nuclear Research and Consultancy Group) Petten, The Netherlands. The polished thick sections were wrapped by commercial Al foils and set into a 99.999 % pure Al holder of 23 mm diameter and 65 mm height in total. The package was Cd-shielded and irradiated with fast neutrons with a flux of 1×10^{13} neutrons per squared centimetre per second for 10 hours. The Fish Canyon Tuff sanidine (age 27.5 Ma; Uto *et al.* 1997; Ishizuka, Yuasa & Uto, 2002) was used as a flux monitor during irradiation to obtain the J values which reflect the degree of neutron activation for the irradiated samples. K_2SO_4 and CaF_2 crystals were also irradiated to correct interference of Ar isotopes produced by the reactions on K or Ca in the samples. The Ar isotope analytical system at Universität Potsdam consists of: (1) a New Wave Gantry Dual Wave laser ablation system with a 50 W CO_2 laser (wavelength 10.6 μm) and 6 mJ UV pulse laser (wavelength 266 nm, frequency-quadrupled) for heating and extracting gas from the samples; (2) an ultra-high vacuum purification line with SAES getters and a cold trap; and (3) a Micromass 5400 noble gas mass spectrometer with a high sensitivity and a ultra-low background. The mass spectrometer has adopted a pulse counting system with an electron multiplier, which effectively works for the analysis of very small amounts of gas. Fish Canyon Tuff sanidine and the K_2SO_4 and CaF_2 crystals were heated by a defocused continuous CO_2 laser beam with a diameter similar to the grain size for 1 min. The unknown samples of the polished thick sections were ablated by the UV pulse laser with 40 μm beam size, 2 min pulsing duration and 10 Hz repetition rate. The extracted gas was exposed to SAES getters and a cold trap, where the metal finger-tube was cooled down to the freezing temperature of ethanol, for 10 min to purify the sample gas to pure Ar gas. Finally, the purified Ar gas was introduced to the noble gas mass spectrometer, Micromass 5400, to determine the Ar isotopic ratios. The Ar isotopic ratios of the sample gas were finally obtained after corrections of blank, mass discrimination by the analytical results of atmospheric argon, interference of the Ar isotopes derived from Ca and K by the irradiation and the decay of the radiogenic Ar isotopes (^{37}Ar and ^{39}Ar) produced by the irradiation. Ages and errors were calculated according to Uto *et al.* (1997), probability plots and isochron calculation and plots for weighted means were produced using the program ISOPLOT (Ludwig, 2009). The data are presented in Table 2. $^{40}Ar/^{39}Ar$ normal and inverse isochrons are depicted in Figure A1 (see the online Supplementary Material available at http://journals.cambridge.org/geo).

4.b. Rb–Sr geochronology

Rb–Sr isotopic data were obtained at GeoForschungsZentrum Potsdam/Germany using a Thermo Scientific Triton thermal ionization mass spectrometer. Sr was measured in dynamic multicollection mode and Rb isotope dilution analysis was performed in static multicollection mode. The value obtained for $^{87}Sr/^{86}Sr$ in the NIST SRM 987 isotopic standard during the period of analytical work was 0.710255 ± 0.000005 ($n = 23$). For age calculation, standard errors of ± 0.005 % for $^{87}Sr/^{86}Sr$ and ± 1.5 % for $^{87}Rb/^{86}Sr$ ratios were assigned to the results, provided that individual analytical uncertainties were smaller than these values. Otherwise, individual analytical uncertainties were used. Handling of mineral separates and analytical procedures are described in more detail in Glodny, Ring & Kühn (2008). Uncertainties of isotope and age data are quoted at 2σ throughout this work. The program ISOPLOT (Ludwig, 2009) was used to calculate regression lines. Decay constants are those recommended by Steiger & Jäger (1977). Analytical data are presented in Table 3.

We analysed white mica in different grain size fractions to check for the possible presence of mixed mica populations, that is, for unequilibrated, detrital, pre- or early-deformational white mica relics (cf. Müller *et al.* 1999), and to detect potentially

https://doi.org/10.1017/S0016756814000508

Table 2. $^{40}Ar^{*}/^{39}Ar$ isotopic ratios and ages of single white mica grains measured by UV laser ablation. Note that errors calculated here for weighted means are given as reduced 1σ error, those given in Figures 1 and 3 are full internal 2σ errors at 95% confidence.

Age	±1σ	$^{40}Ar^{*}/^{39}Ar_{K}$	±1σ	$^{40}Ar/^{39}Ar$	±1σ	$^{38}Ar/^{39}Ar$	±1σ	$^{37}Ar/^{39}Ar$	±1σ	$^{36}Ar/^{39}Ar$ ($\times10^{-3}$)	±1σ	$^{40}Ar_{atm}$ (%)	K/Ca		
Lab ID U12002: 10Ca11, J:0.002506, Felsic metavolcanic Fourchu Group															
328.06	95.47	79.580	23.160	273.334	11.845	0.075	0.024	0.262	0.015	0.667	0.070	70.885	0.489	normal isochron age:	404 ± 71 Ma
372.04	42.56	91.391	10.454	223.604	7.338	0.092	0.014	0.091	0.010	0.455	0.028	59.128	1.401	MSWD	0.31
395.46	24.57	97.798	6.077	156.459	4.223	0.041	0.008	0.030	0.003	0.202	0.016	37.491	4.298	initial $^{40}Ar/^{36}Ar$ ratio:	280 ± 56
405.44	84.18	100.554	20.877	323.697	16.264	0.159	0.028	0.388	0.018	0.768	0.057	68.935	0.330	inverse isochron age:	402 ± 70 Ma
387.89	18.17	(weighted mean)												MSWD	0.31
														initial $^{40}Ar/^{36}Ar$ ratio:	283 ± 55
Lab ID U12001: 10Ca34, J:0.002506, Felsic metavolcanic Fourchu Group															
332.09	17.81	80.651	4.725	142.111	2.687	0.039	0.006	0.077	0.003	0.212	0.014	43.246	1.665		
342.72	22.99	83.485	6.140	161.467	2.923	0.059	0.009	0.124	0.005	0.269	0.019	48.294	1.037	normal isochron age:	351 ± 20 Ma
343.25	43.53	83.628	11.642	241.152	6.128	0.117	0.025	0.179	0.007	0.542	0.035	65.321	0.728	MSWD	1.09
350.19	69.65	85.486	18.703	364.568	12.305	0.189	0.021	0.458	0.022	0.961	0.055	76.551	0.285	initial $^{40}Ar/^{36}Ar$ ratio:	302 ± 11
358.62	14.26	87.756	3.833	184.941	2.834	0.073	0.008	0.084	0.005	0.335	0.011	52.548	1.525	inverse isochron age:	356 ± 20 Ma
381.44	12.27	93.952	3.333	150.970	1.789	0.048	0.005	0.042	0.002	0.196	0.010	37.766	3.140	MSWD	1.11
408.79	42.83	101.485	11.877	223.224	6.395	0.073	0.017	0.176	0.009	0.419	0.035	54.536	0.732	initial $^{40}Ar/^{36}Ar$ ratio:	302 ± 11
410.18	52.84	101.870	14.666	582.715	5.877	0.329	0.036	0.449	0.021	1.655	0.052	82.518	0.291		
418.59	68.34	104.210	19.059	997.194	19.954	0.634	0.053	0.195	0.014	3.072	0.089	89.550	0.669		
363.30	7.36	(weighted mean)													
Lab ID U12009: 10Ca37, J:0.002505, Felsic metavolcanic, East Bay Hills Group															
386.57	3.70	95.395	0.941	105.238	0.606	0.021	0.002	0.005	0.002	0.034	0.003	9.349	22.581	normal isochron age:	385 ± 6.3 Ma
390.22	3.15	96.398	0.775	102.409	0.330	0.016	0.001	0.012	0.001	0.021	0.002	5.866	10.083	MSWD	1.90
390.98	4.70	96.605	1.232	106.01	0.942	0.025	0.002	0.005	0.001	0.032	0.003	8.867	25.053	initial $^{40}Ar/^{36}Ar$ ratio:	347 ± 38
400.57	3.42	99.248	0.857	112.246	0.475	0.023	0.001	0.002	0.001	0.045	0.003	11.576	47.403	inverse isochron age:	386 ± 6.2 Ma
408.97	7.43	101.575	2.022	145.299	0.940	0.040	0.003	0.049	0.003	0.151	0.006	30.090	2.350	MSWD	1.90
393.30	1.76	(weighted mean 1)												initial $^{40}Ar/^{36}Ar$ ratio:	348 ± 37
Lab ID U12009: 10Ca37, J:0.002505, Felsic metavolcanic, East Bay Hills Group															
423.29	4.57	105.565	1.208	126.68	0.875	0.037	0.002	0.013	0.002	0.073	0.003	16.664	8.804	normal isochron age:	406 ± 17 Ma
423.84	4.85	105.719	1.289	119.252	0.597	0.024	0.001	0.012	0.002	0.047	0.004	11.345	9.706	MSWD	2.30
435.08	4.51	108.876	1.193	131.522	0.812	0.030	0.001	0.014	0.001	0.078	0.003	17.216	8.040	initial $^{40}Ar/^{36}Ar$ ratio:	384 ± 70
427.61	2.68	(weighted mean 2)												inverse isochron age:	407 ± 16 Ma
														MSWD	2.30
														initial $^{40}Ar/^{36}Ar$ ratio:	384 ± 65
Lab ID U12006: 10Ca42, J:0.002505, Felsic metavolcanic, East Bay Hills Group															
380.92	3.04	93.850	0.750	102.178	0.290	0.011	0.001	0.001	0.001	0.029	0.002	8.146	169.875	normal isochron age:	384.1 ± 10 Ma
382.36	2.76	94.242	0.681	108.916	0.432	0.033	0.002	0.000	0.001	0.050	0.002	13.469	290.330	MSWD	2.30
384.63	11.83	94.864	2.918	173.582	1.934	0.068	0.005	0.040	0.004	0.271	0.010	45.348	3.001	initial $^{40}Ar/^{36}Ar$ ratio:	307 ± 64
385.30	5.35	95.048	1.319	118.720	0.825	0.015	0.004	0.025	0.002	0.081	0.004	19.936	4.753	inverse isochron age:	382.8 ± 9.6 Ma
386.50	5.78	95.376	1.427	104.805	0.823	0.024	0.002	0.009	0.001	0.032	0.004	8.992	13.798	MSWD	2.40
393.45	3.47	97.285	0.858	107.604	0.856	0.025	0.001	0.006	0.000	0.035	0.001	9.586	21.194	initial $^{40}Ar/^{36}Ar$ ratio:	312 ± 23
421.17	33.66	104.972	8.391	224.065	7.643	0.068	0.020	0.030	0.007	0.410	0.029	53.150	4.088		
385.16	1.58	(weighted mean)													

Table 2. Continued.

Age	±1σ	$^{40}Ar^*/^{39}Ar_K$	±1σ	$^{40}Ar/^{39}Ar$	±1σ	$^{38}Ar/^{39}Ar$	±1σ	$^{37}Ar/^{39}Ar$	±1σ	$^{36}Ar/^{39}Ar$ ($\times10^{-3}$)	±1σ	$^{40}Ar_{atm}$ (%)	K/Ca		
Lab ID U12024: 11Ca15, J:0.002531, Felsic volcanoclastic metasediment, Pringle Mountain Group															
372.31	2.88	90.56194	0.6866	115.411	0.512	0.032	0.003	0.003	0.001	0.084	0.002	21.527	1.530		
														normal isochron age:	396.1 ± 7 Ma
395.12	3.95	96.741	1.005	144.467	1.061	0.048	0.002	0.002	0.001	0.162	0.003	33.033	1.685	MSWD	1.4
395.86	2.25	96.94267	0.4748	114.783	0.467	0.022	0.002	0.001	0.001	0.060	0.001	15.538	4.753	initial $^{40}Ar/^{36}Ar$ ratio:	295 ± 21
400.99	4.81	98.34322	1.2548	125.955	1.524	0.031	0.003	0.001	0.002	0.094	0.002	21.918	25.050	inverse isochron age:	396.5 ± 7 Ma
396.30	1.60	(weighted mean 1)												MSWD	1.2
														initial $^{40}Ar/^{36}Ar$ ratio:	295 ± 21
Lab ID U12024: 11Ca15, J:0.002531, Felsic volcanoclastic metasediment, Pringle Mountain Group															
413.54	2.58	101.789	0.584	121.875	0.595	0.023	0.001	0.000	0.001	0.068	0.001	16.477	19.970	normal isochron age:	418 ± 15 Ma
417.32	4.83	102.829	1.267	159.809	1.512	0.052	0.003	0.002	0.002	0.193	0.003	35.652	2.499	MSWD	5.60
421.54	1.91	103.9956	0.3266	114.739	0.289	0.020	0.001	0.002	0.001	0.036	0.001	9.3579	1.971	initial $^{40}Ar/^{36}Ar$ ratio:	296 ± 65
445.59	11.94	110.694	3.318	275.020	2.889	0.124	0.009	0.006	0.002	0.556	0.012	59.750	0.714	inverse isochron age:	414 ± 21 Ma
419.70	1.20	(weighted mean 2)												MSWD	7.60
														initial $^{40}Ar/^{36}Ar$ ratio:	308 ± 33
Lab ID U12024: 11Ca15, J:0.002531, Felsic volcanoclastic metasediment, Pringle Mountain Group															
474.88	3.89	118.973	1.002	222.205	0.731	0.093	0.003	0.003	0.001	0.349	0.003	46.456	1.278	normal isochron age:	449 ± 40 Ma
477.12	6.39	119.6111	1.7582	256.930	2.665	0.103	0.006	0.001	0.001	0.464	0.006	53.445	5.850	MSWD	1.90
496.88	10.31	125.280	2.932	272.938	2.888	0.136	0.002	0.004	0.002	0.500	0.010	54.099	1.066	initial 40Ar/36Ar ratio:	316 ± 29
477.20	3.40	(weighted mean 3)												inverse isochron age:	449 ± 40 Ma
														MSWD	2.10
														initial 40Ar/36Ar ratio:	316 ± 28
Lab ID U13001: 11Ca18, J:0.002539, Felsic volcanoclastic metasediment, Pringle Mountain Group															
434.71	4.25	107.313	1.099	121.503	1.023	0.020	0.002	0.001	0.002	0.048	0.002	11.674	2.983		
434.43	3.50	107.237	0.874	116.134	0.711	0.018	0.001	0.048	0.002	0.033	0.002	7.656	0.084	inverse isochron age:	445 ± 6.2 Ma
437.45	4.45	108.077	1.161	122.268	1.116	0.022	0.001	0.004	0.001	0.048	0.002	11.602	0.919	MSWD	1.40
442.22	2.42	109.404	0.513	114.583	0.457	0.021	0.001	0.000	0.001	0.018	0.001	4.514	18.698	initial 40Ar/36Ar ratio:	235 ± 58
438.60	1.65	(weighted mean 1)													
Lab ID U13001: 11Ca18, J:0.002539, Felsic volcanoclastic metasediment, Pringle Mountain Group															
451.16	3.52	111.905	0.879	115.712	0.884	0.015	0.001	0.001	0.001	0.013	0.001	3.285	6.004	normal isochron age:	463 ± 10 Ma
460.39	3.79	114.497	0.963	123.067	0.910	0.017	0.002	0.000	0.001	0.029	0.002	6.958	12.473	MSWD	1.14
464.40	7.21	115.629	1.983	137.680	1.837	0.032	0.003	0.001	0.002	0.075	0.004	16.012	5.604	initial $^{40}Ar/^{36}Ar$ ratio:	290 ± 75
473.29	5.21	118.147	1.401	118.411	1.395	0.001	0.000	0.000	0.000	0.001	0.000	0.217	21.280	inverse isochron age:	468 ± 7.8 Ma
464.80	2.85	(weighted mean 2)												MSWD	3.30
														initial $^{40}Ar/^{36}Ar$ ratio:	259 ± 61
525.27	4.52	133.535	1.213	226.316	0.471	0.079	0.002	0.001	0.001	0.314	0.004	40.995	7.853		

Table 3. Rb–Sr analytical data and isotopic ratios; m – current range (Å) on a magnetic separator at which a certain fraction of white mica is magnetic; wm – grain size of white mica fraction (μm).

Analysis no.	Material	Rb (ppm)	Sr (ppm)	$^{87}Rb/^{86}Sr$	$^{87}Sr/^{86}Sr$	$^{87}Sr/^{86}Sr$ $2\sigma_m$ (%)
11Ca05 (364.6 ± 8.4 Ma, MSWD = 2.1, Sr_i = 0.703577 ± 0.000031)						
PS1896	m = 0.35 (epidote rich)	6.16	511	0.0348	0.703732	0.0010
PS1898	m = 0.5–0.8, wm = 200–160	24.1	237	0.295	0.705130	0.0013
PS1899	m = 0.5–0.8, wm = 160–9	16.9	226	0.216	0.704704	0.0019
PS1943	m = 0.5–0.8, wm < 90	9.65	240	0.116	0.704204	0.0013
PS1942	m = 0.5–0.8, wm = 355–250	25.6	232	0.319	0.705227	0.0008
PS1941	m = 0.5–0.8, wm = 250–200	26.6	226	0.340	0.705367	0.0022
PS1897	albite	7.38	51.6	0.414	0.705680	0.0040
11Ca13 (388.6 ± 6.9 Ma, MSWD = 0.3, Sr_i = 0.71450 ± 0.00050)						
PS1900	albite	87.7	76.9	3.31	0.732824	0.0015
PS1901	m = 0.3, leach (chlorite rich)	103	51.9	5.79	0.746375	0.0014
PS1902	m = 0.8, wm = 160–90	225	50.5	13.0	0.786531	0.0016
PS1949	m = 0.8, wm <90	151	67.6	6.48	0.750298	0.0007

Table 4. Fission track ages of zircon

Sample	*N*	Track density ($\times 10^6$ tr cm^{-2}) Ps (Ns)	Pi (Ni)	Pd (Nd)	Age dispersion (Pχ2)	Central age (Ma) (±1σ)
10Ca18	13	12.85 (1488)	1.856 (215)	0.5513 (3529)	<0.01% (99%)	227.0 ± 18.2
10Ca29	7	16.46 (727)	2.332 (103)	0.5498 (3519)	<0.01% (97%)	230.8 ± 25.5
10Ca36	3	19.71 (164)	2.764 (23)	0.5483 (3509)	<0.01% (82%)	232.5 ± 52.3
10Ca37	10	13.77 (2009)	1.775 (259)	0.5258 (3365)	<0.01% (99%)	242.3 ± 18.0
10Ca40	6	53.03 (465)	1.106 (97)	0.5228 (3346)	10.85% (34%)	150.9 ± 18.9
10Ca43	10	12.06 (996)	1.744 (144)	0.5468 (3500)	<0.01% (95%)	225.0 ± 21.4

protracted (re)crystallization or deformation histories of the samples.

4.c. Zircon fission track geochronology

Zircon crystals were separated, mounted, polished and etched according to the techniques outlined by Thomson & Ring (2006). The samples were analysed applying the external detector method and irradiated at the Oregon State University Triga Reactor, Corvallis, USA. The neutron fluence for zircon was monitored using the Institute for Reference Materials and Measurements (IRMM) uranium-dosed IRMM-541 glass. Spontaneous and induced fission track (FT) densities were counted using an Olympus BX51 microscope at 1250× magnification. Central ages (Galbraith & Laslett, 1993) were calculated using the IUGS recommended Zeta-calibration approach of Hurford & Green (1983), which allows for non-Poissonian variation within a population of single-grain ages belonging to an individual sample. The χ^2 test indicates the probability that all grains counted belong to a single population of ages. A probability of less than 5 % is taken as evidence for a significant spread of single-grain ages. A spread in individual grain ages can result either from inheritance of detrital grains from mixed source areas, or from differential annealing in grains of different composition by heating within a narrow range of temperatures (Green *et al.* 1989). An IRMM-541 zeta calibration factor of 121.1 ± 3.5 was obtained by repeated calibration against a number of internationally agreed age standards according to the recommendations of Hurford (1990). Data are presented in Table 4 (see also Table A1 in the online Supplementary Material available at http://journals.cambridge.org/geo) and Figure 5. Probability plots were produced with the program ISOPLOT (Ludwig, 2009) and radial plots with the software RadialPlotter (Vermeesch, 2009).

5. Sample description and geochronological results

5.a. $^{40}Ar/^{39}Ar$ dating of white mica

Six samples were selected for $^{40}Ar/^{39}Ar$ dating, four from the NW and SE parts of the Mira terrane and two from the Sporting Mountain area in the SW part (Table 2; Figs 1, 3).

The four samples (10Ca11, 10Ca34, 10Ca37 and 10Ca42) from the NW and SE parts of the terrane are strongly foliated and sheared felsic metavolcanic rocks, interpreted to have been deformed in the D_2 event. They contain the metamorphic mineral assemblage phengite-epidote-chlorite-albite-quartz-titanite. Bands enriched in strongly oriented white mica (and more rarely chlorite) due to pressure solution at quartz/feldspar-phyllosilicate interfaces vary at millimetre to centimetre scale with only a few laminae still showing recognizable relict fabrics such as porphyritic and/or pyroclastic textures (Fig. 2a, b). Hence a strong strain gradient is apparent at microscale. Albitic plagioclase phenocrysts and clasts (0.1–2 mm in size) are abundant as rotated relicts between phyllosilicate bands (σ-clasts) showing considerable brittle internal deformation (Fig. 2a, b). Plagioclase is commonly sericitized, containing clusters of undeformed fine-grained white mica with grain sizes of 5–30 μm (Fig. 2a). At the rims of porphyroclasts, white mica is more abundant and

https://doi.org/10.1017/S0016756814000508

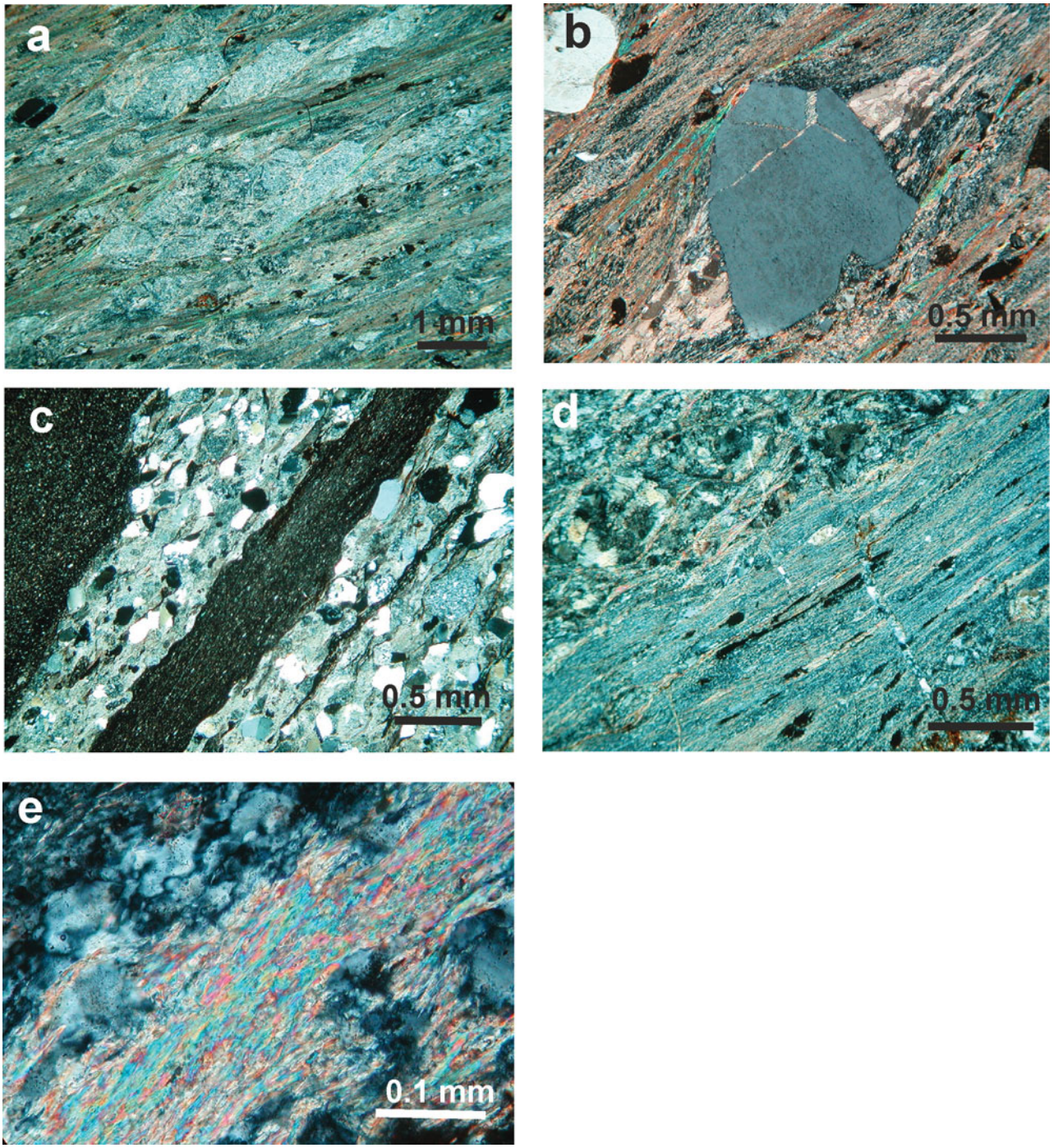

Figure 2. Micrographs (all crossed polars): (a) σ-clast of plagioclase with brittle internal deformation and crystallization of white mica clusters (sample 10Ca37); (b) σ-clast containing an internally undeformed quartz phenocryst showing a resorption embayment and white mica filled fissures (sample 10Ca37); (c) two oriented slate clasts in a matrix of undeformed mineral clasts in a pyroclastic rock (sample 11Ca18); (d) bands with strongly oriented white mica including quartz and feldspar clasts oriented due to pressure solution (sample 11Ca13); and (e) recrystallization of large white mica in an oriented cluster of fine-grained white mica and recrystallization of quartz (sample 11Ca13).

grain size increases up to 100 μm (Fig. 2b). In low-strain laminae, quartz also occurs as primary phenocrysts with corrosion embayments (0.5–1 mm), both with and without minor subgrain formation (Fig. 2b). Fissures are filled by white mica or calcite. Incipient recrystallization of quartz towards a polygonal fabric occurs in the matrix, in fissure fillings and especially in pressure shadows (0.01–0.05 mm). All four of these samples were included in the determination of peak metamorphic conditions in the range of 3.5 ± 0.4 kbar and 280 ± 30 °C for the Mira terrane on the basis of mineral composition (Willner *et al.* 2013*b*). Based on data reported by Willner *et al.* (2013*b*), composition of the white mica varies from muscovite to phengite (Si 3.1 to 3.4 atoms per formula unit).

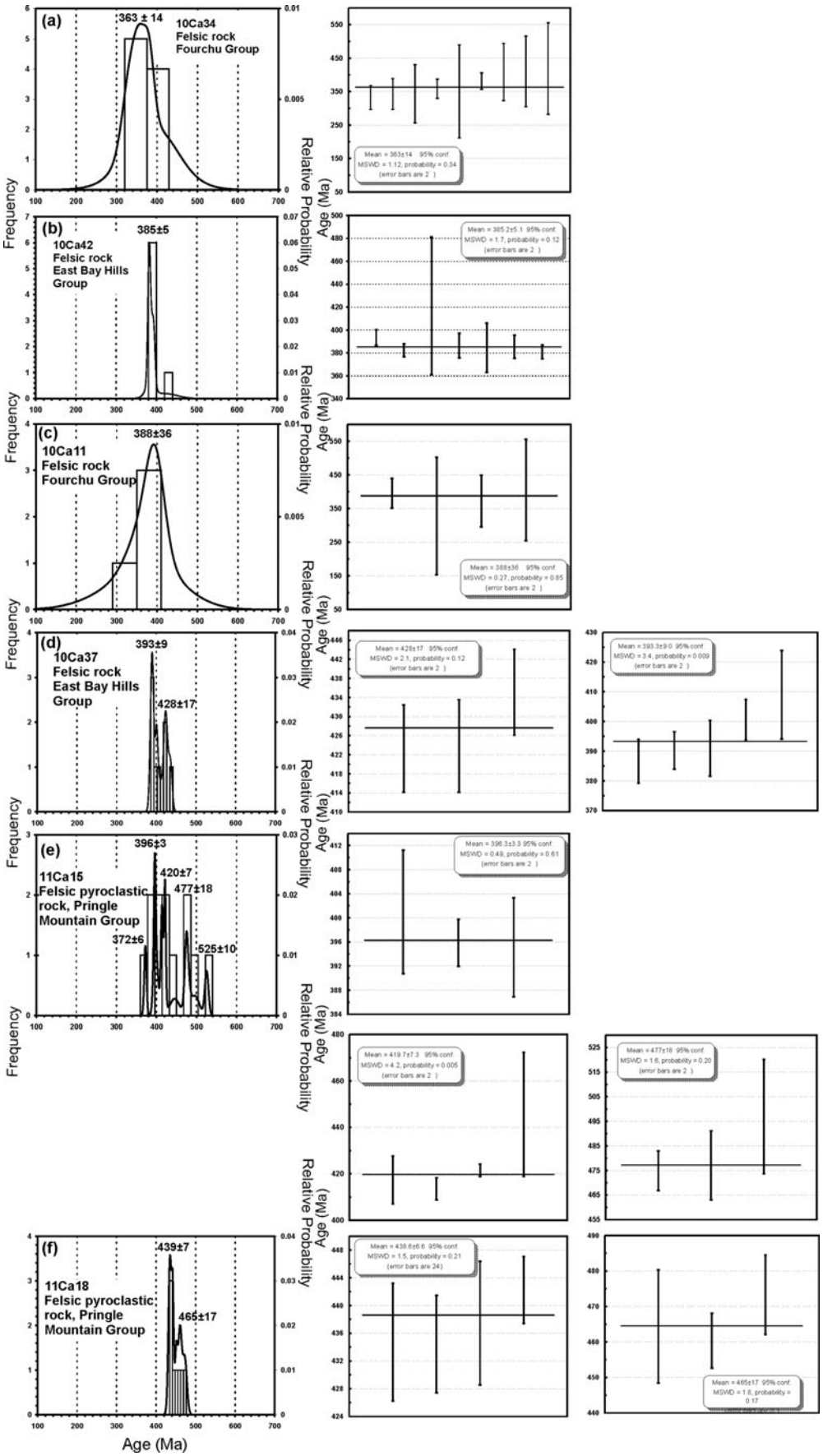

Figure 3. (a–f) Left: cumulative probability plots for $^{40}Ar/^{39}Ar$ single-grain laser ablation ages of white mica from rocks of the Mira terrane; (a–f) right: respective weighted mean plots.

https://doi.org/10.1017/S0016756814000508

Spot ages of white mica were obtained by laser ablation with 40 μm spot diameter both in high-strain laminae with enriched white mica and in white mica clusters in sericitized plagioclase in low-strain laminae. Only a few (2–4) adjacent grains were analysed, in contrast to conventional step heating of concentrates of multiple grains. Chlorite was not present in the dated clusters. A similar age range was detected among samples as given by the weighted means of the single spot ages (errors are 2σ; Table 2; Figs 1, 3): 388 ± 36 Ma (10Ca11; $n = 4$); 363 ± 14 Ma (10Ca34; $n = 9$); 393 ± 9 Ma (10Ca37; $n = 5$); and 385 ± 5 Ma (10Ca42; $n = 7$). These ages are corroborated by ages from normal and inverse isochrons which overlap the weighted means within 2σ confidence intervals (Table 2; see also online Supplementary Material Fig. E1, available at http://journals.cambridge.org/geo): 404 ± 71 Ma and 402 ± 70 Ma (sample 10Ca11); 351 ± 20 Ma and 356 ± 20 Ma (sample 10Ca34); 385 ± 6.2 Ma and 386 ± 6.3 Ma (sample 10Ca37); and 384 ± 10 Ma and 383 ± 10 Ma (sample 10Ca42). In three of the samples, the initial $^{40}Ar/^{36}Ar$ ratios of 280 ± 56 and 283 ± 55 (sample 10Ca11), 302 ± 11and 302 ± 11 (sample 10Ca34) and 307 ± 64 and 312 ± 23 (sample 10Ca42) overlap those of atmospheric Ar (295.5; Table 2; Fig. E1, available at http://journals.cambridge.org/geo), indicating that the presence of excess Ar is unlikely. The fourth sample 10Ca37 has slightly higher initial $^{40}Ar/^{36}Ar$ ratios of 347 ± 37 and 348 ± 38 (Table 2) and is the only sample in which significant age differences were detected at the 2σ level at thin-section scale, and hence which might contain some inherited (excess) Ar. A spot age peak of 428 ± 17 Ma (weighted mean of three spot ages) was measured in sericitic white mica clusters in plagioclase within low-strain domains, consistent with the normal and inverse isochron ages within 2σ errors (406 ± 35 Ma and 407 ± 32 Ma). The initial $^{40}Ar/^{36}Ar$ ratios of 384 ± 140 and 384 ± 130 also coincide with atmospheric Ar within their large 2σ errors (Table 2).

The two other dated samples (11Ca15, 11Ca18) are felsic volcanoclastic or metasedimentary rocks from the Pringle Mountain Group in the Sporting Mountain belt (Fig. 1). Metamorphic conditions in the Sporting Mountain belt fall within the range of the remainder of the Mira terrane based on a sample collected from the NW part of the belt (Willner *et al.* 2013*b*). The SE and likely NW margins of that belt are major shear zones, but the sampled areas appear to have been little or not-at-all affected by shear zones. The dated samples are weakly to moderately cleaved and display incipient recrystallization of quartz in the matrix. They contain slate clasts which are now oriented parallel to the predominant foliation, and the grain size of white mica in the clasts increases at the rims (Fig. 2c). Some veins filled with white mica intersect the foliation.

Sample 11Ca15 yielded a wide spectrum of white mica spot ages (Fig. 3). A dominant age peak (weighted mean; 2σ errors) at 396 ± 3 Ma is defined by only 3 spot ages (normal isochron age 396 ± 7 Ma; inverse isochron age 397 ± 7 Ma; both initial $^{40}Ar/^{36}Ar$ ratios 295 ± 21; Table 2) and a single spot yielded an age of 372 ± 6 Ma. Only these ages are similar to those from the four samples previously described. Three older apparent age peaks occur at 420 ± 7 Ma ($n = 4$), 477 ± 18 Ma ($n = 3$) and 525 ± 10 Ma ($n = 1$). These ages were measured in the slate clasts as well as in matrix white mica clusters. The weighted means of single age clusters do not overlap within 2σ errors, and are consistent with ages derived from the respective normal and inverse isochrons within 2σ errors (Table 2; Fig. E1, available at http://journals.cambridge.org/geo). The respective initial $^{40}Ar/^{36}Ar$ ratios (296 ± 65 and 308 ± 33; 316 ± 29 and 316 ± 28) are comparable to that of atmospheric Ar within 2σ errors (Table 2). Excess Ar does not appear to be present in sample 11Ca15.

In sample 10Ca18 three apparent age peaks were detected, none of which is Devonian: 439 ± 7 Ma ($n = 4$), 451 ± 14 Ma ($n = 1$) and 465 ± 17 Ma ($n = 3$). The first weighted mean is consistent with the inverse isochron age (445 ± 6 Ma; Table 2), and the third with both the normal and inverse isochron ages (463 ± 10 Ma and 468 ± 8 Ma; Table 2). The initial $^{40}Ar/^{36}Ar$ ratios (235 ± 58, 290 ± 75 and 259 ± 61; Table 2) are identical to that of atmospheric Ar within 2σ errors, indicating that the presence of excess Ar is unlikely.

The Sporting Mountain belt samples show strong age heterogeneity both at thin-section scale and between outcrops (i.e. between the two samples), and probably preserve inherited ages. The lack of evidence for a D_2 overprint in this area can explain the scarcity (in sample 11Ca15) or lack (in sample 10Ca18) of Middle–Late Devonian ages characteristic of the other four dated samples.

5.b. Rb–Sr mineral isochrons

Two samples, both from areas with prominent D_2 sinistral strike-slip deformation, were analysed for Rb–Sr mineral systematics: mafic metavolcanic sample 11Ca05 and felsic metavolcanic sample 11Ca13 (Table 3; Figs 1, 4). In both samples white mica is too fine grained to be conventionally separated as individual crystals, and intimately intergrown with the matrix phases. We therefore separated mica-rich aggregates magnetically and split these aggregates into sieve fractions. Analysed white mica-rich fractions for the Rb–Sr mineral isochrons differ in grain size and in amount and type of admixture, that is, quartz, chlorite, epidote and feldspar. In both samples a pure albite fraction was obtained, and in sample 11Ca05 an almost-pure epidote fraction.

Sample 11Ca05 is likely of pyroclastic origin and dominated by chlorite and epidote. It is slightly foliated and white mica is mainly in 0.5–1 mm clusters parallel to the foliation. A few recrystallized individual grains are up to 100 μm in size. The isochron is defined by seven fractions including one albite fraction, two white mica fractions and four mixed fractions, yielding an age

https://doi.org/10.1017/S0016756814000508

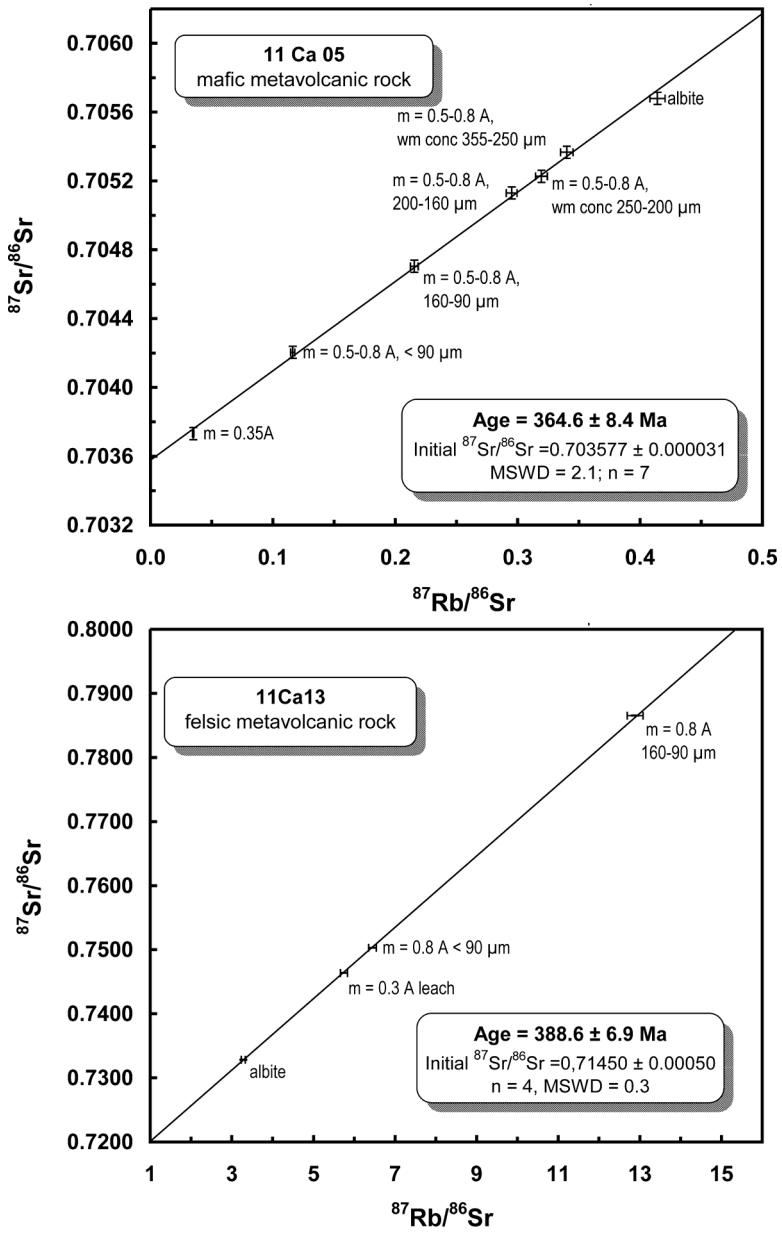

Figure 4. Rb–Sr mineral isochrons for two samples from the Mira terrane: data-point error crosses are 2σ; m – current range (Å) on a magnetic separator at which a certain fraction is magnetic.

of 364.6 ± 8.4 Ma. This age is the same as the $^{40}Ar/^{36}Ar$ white mica age of 363 ± 14 Ma from sample 10Ca34 from the same locality.

Sample 11Ca13 is dominated by albite, quartz and white mica. It is strongly foliated with a pronounced non-coaxial fabric (σ-clasts, s-c-fabric) and pressure solution. White mica is oriented parallel to the s-c fabric, and the foliation is crossed by fissures filled by white mica (Fig. 2d). Recrystallization of large white mica in oriented clusters of fine-grained white mica and incipient recrystallization of quartz towards a polygonal fabric in the matrix is prominent (Fig. 2e). The isochron is defined by four fractions including an albite fraction and three mixed fractions containing white mica, and yields an age of 388.6 ± 6.9 Ma. This age is similar to the $^{40}Ar/^{36}Ar$ white mica age of 385 ± 5 Ma from nearby sample 10Ca42.

5.c. Fission track dating of zircon

Fission tracks were analysed in zircon concentrates from six samples collected from locations throughout the Mira terrane (Fig. 1), including two volcanogenic metasandstone samples (10Ca36, 10Ca40), a felsic metavolcanic sample (10Ca37), a volcanoclastic metasedimentary rock (10Ca40), a granite cobble in a metaconglomerate (10Ca43) and a quartzite sample from the Cambrian cover sequence (10Ca18).

Although single FT ages vary widely between 280 and 158 Ma, the resulting central ages (see Section 4.3; Figs 1, 5; Table 4) yield a more restricted age range between 242 and 225 Ma: 225 ± 21 Ma (10Ca42; n = 6); 227 ± 18 Ma (10Ca18; n = 13); 231 ± 26 Ma (10Ca29; n = 7); 232 ± 52 (10Ca36; n = 3); and 242 ± 18 Ma (10Ca37; n = 10). They show no variation with rock type or with the $^{40}Ar/^{39}Ar$ white mica

https://doi.org/10.1017/S0016756814000508

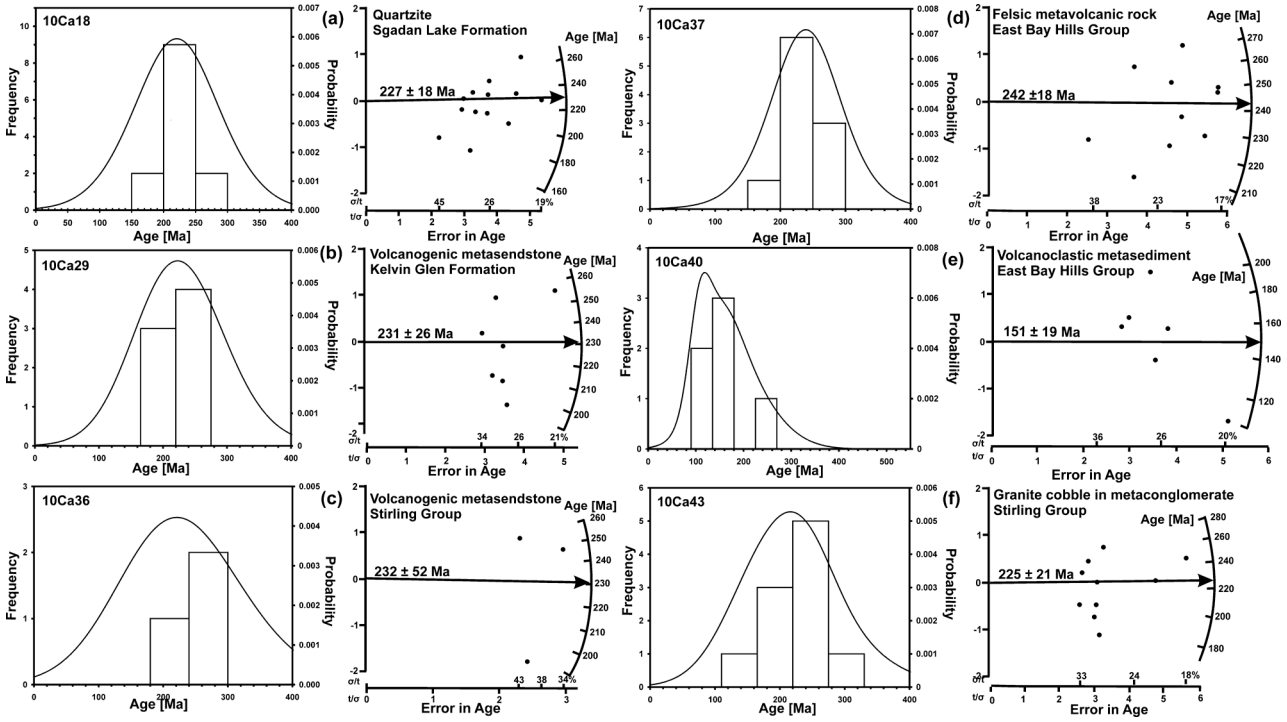

Figure 5. Combined relative probability plot/histogram (left row) and radial plot representation (right row) of zircon single-grain fission-track age data for selected rocks of the Mira terrane.

and Rb–Sr mineral isochron ages, and are similar to one another within the large 2σ range. An exception is sample 10Ca40 ($n = 6$) with a much younger age spectrum of single ages between 230 and 107 Ma and a central age of 151 ± 19 Ma.

6. Discussion

6.a. Age of regional metamorphism and deformation

The $^{40}Ar/^{39}Ar$ age of crystallization of metamorphic white mica in samples 10Ca11, 10Ca34, 10Ca37 and 10Ca42, all with strong D_2 overprint, is Middle–Late Devonian, that is, it ranges between 393 ± 9 Ma and 363 ± 14 Ma. This age spectrum is coincident with ages of Rb–Sr mineral isochron ages determined in samples 11Ca05 and 11Ca13 at 365 ± 7 Ma and 389 ± 8 Ma, respectively, both of which also have a strong D_2 overprint. Because mineral assemblages are dated with Rb–Sr mineral isochrons, this similarity in ages indicates that Sr-isotopic equilibrium at hand specimen scale was attained in rocks that had also achieved microchemical equilibrium.

Willner *et al.* (2013*b*) attributed the microchemical equilibration to very low- to low-grade regional metamorphism, characterized by conditions of 3.5 ± 0.4 kbar and 280 ± 30 °C which they corroborated in samples from Neoproterozoic metavolcanic-metasedimentary belts throughout the Mira terrane. According to Willner *et al.* (2013*b*), the varying compositions of the metamorphic phases at thin-section scale originated during continuously new nucleation of phases during changing *P–T* conditions along the late prograde and likely early retrograde *P–T* path, a kinetic phenomenon characteristic of very low- and low-grade metamorphism. During metamorphism water was present between reactants and reaction products, which mainly precipitated in clusters. As a result, transient equilibrium conditions were present throughout this partial *P–T* path. Equilibrium conditions are now further corroborated by the Sr-isotopic equilibrium observed at hand specimen scale. The maximum possible change in *P–T* conditions (*c.* 50 °C, *c.* 1 kbar) during growth of white mica (Willner *et al.* 2013*b*) probably occurred in the time recorded by the single Rb–Sr ages and their 2σ errors, that is, within *c.* 15 Ma. In the four samples which record only Middle–Late Devonian ages (10Ca11, 10Ca34, 10Ca42 and 11Ca05), any older white mica, if present, has been entirely recrystallized. The metamorphic white mica evidently grew and/or recrystallized during deformation and mylonitization related to the formation of prominent ductile sinistral D_2 shear zones. The associated metamorphic overprint was pervasive, because mica clusters replacing undeformed parts of feldspar also have the same Devonian age.

The occurrence of very low-grade metamorphic minerals in the Neoproterozoic volcanic-sedimentary-plutonic belts of the Mira terrane was previously ascribed to a pervasive hydrothermal alteration event around 560–550 Ma, detected by depletion in $\delta^{18}O$ which characterizes the Avalonian terranes in the northern Applachian orogen (Potter, Longstaffe & Barr, 2008; Potter *et al.* 2008). No such ages were detected in our samples, although they have commonly been recorded in detrital white mica in Cambrian cover

https://doi.org/10.1017/S0016756814000508

sequences in West Avalonia, including the Mira terrane (Reynolds, Barr & White, 2009; Barr *et al.* 2014). However, detrital white mica grains are at least an order of magnitude larger than the metamorphic white mica grains in our samples. The metamorphic white mica grains experienced complete or nearly complete re-equilibration during Middle–Late Devonian time, likely related to the fact that they were strongly affected by D_2 as a result of concomitant infiltration and channelling of a hydrous metamorphic fluid through the shear zones. Massonne & Willner (2008) and Willner *et al.* (2013*b*) showed that maximum dehydration under regional metamorphic conditions occurs at 250–350 °C depending on pressure. Influx of these internally generated metamorphic fluids would not likely have affected the $\delta^{18}O$ anomaly which, by contrast, was originally produced by an influx of external meteoric fluids (Potter, Longstaffe & Barr, 2008; Potter *et al.* 2008).

An additional concomitant Devonian event in the Mira terrane was the high-level intrusion of a few small granitic bodies (Fig. 1) in the likely age range 380–370 Ma (Barr & Macdonald, 1992; Bevier *et al.* 1993). Potential resetting by fluids generated during this event (magmatic H_2O release; small-scale hydrothermal convection) appears to have been rather insignificant as a cause for the ubiquitous Devonian $^{40}Ar/^{39}Ar$ ages at the locations sampled for this study although, in some areas, contact metamorphic overprinting and skarn development were widespread (Macdonald & Barr, 1993*b*).

6.b. Possible Silurian and Ordovician relict ages

The $^{40}Ar/^{39}Ar$ age spectra in samples 10Ca37, 11Ca05 and 11Ca13 display inhomogeneous distribution of spot ages at thin-section scale and between outcrops. These spot ages do not display a continuum, as would be expected if they were recording partial resetting of older ages. Instead they cluster around three age peaks: 420–428 Ma, 439 Ma and 465–477 Ma. These possible relict age peaks are similar within error to the respective normal and inverse isochron ages, and the respective initial $^{40}Ar/^{36}Ar$ ratios are comparable to that of atmospheric Ar within 2σ errors (Table 2), indicating that the presence of inherited (excess) Ar is unlikely. Detrital slate clasts in samples 11Ca15 and 11Ca18 or white mica formed during the pervasive hydrothermal fluid influx around 560–550 Ma (Potter, Longstaffe & Barr, 2008; Potter *et al.* 2008; Reynolds, Barr & White, 2009) could be sources for inherited Ar.

Detrital white mica grains from relatively undeformed sandstone of the Lower Cambrian Bengal Road Formation yielded continuous spectra at *c.* 550–634 Ma with separate minor peaks at 530 Ma and 469 Ma (Reynolds, Barr & White, 2009). Similar ages were obtained from time-equivalent units in New Brunswick, leading Reynolds, Barr & White (2009) to interpret the age spectra as representing a 650–630 Ma proximal detrital source and a resetting event at *c.* 560–550 Ma. The resetting event was postulated to have been a hydrothermal overprint which may also have produced the pervasive $\delta^{18}O$ depletion in Avalonia during the early stages of transtension-related rifting (Potter, Longstaffe & Barr, 2008; Potter *et al.* 2008).

On the other hand, collision of Avalonia with the leading edge of composite Laurentia (including previously accreted Ganderia) and subsequent related deformation, crustal thickening and metamorphism after closure of the Acadian seaway occurred during the late Silurian – Early Devonian Acadian orogeny between about 421 and 395 Ma, according to several lines of evidence from the collision zones in New Brunswick and Newfoundland (e.g. Murphy, van Staal & Keppie, 1999; White *et al.* 2006; van Staal *et al.* 2009; van Staal & Barr, 2012). Water released during early Acadian burial could have been responsible for the 420–428 Ma $^{40}Ar/^{39}Ar$ spot age peaks detected as relicts in two of the Mira terrane samples (10Ca37 and 11Ca15). More significant is the $^{40}Ar/^{39}Ar$ white mica age of 396 ± 3 Ma for sample 11Ca15, which could be interpreted to reflect growth of white mica in S_1 given that the area around this sample was not noticeably affected by D_2. If correct, a progressive D_1–D_2 transpressive deformation event may have started during late Early Devonian time. This timing suggests that the event was linked to either the end stages of the Acadian orogeny or the onset of the Neoacadian orogeny. In any case, it is clear that a larger database is needed to corroborate the relict $^{40}Ar/^{39}Ar$ spot age peaks and investigate whether they correspond to fluid influx related to known geological processes or represent incomplete resetting of Neoproterozoic–Cambrian ages by Devonian events.

6.c. Devonian transpressive deformation

The Devonian $^{40}Ar/^{39}Ar$ spot ages and Rb–Sr ages reported here are interpreted to date prominent sinistral strike-slip deformation in the Mira terrane, although the oldest Devonian $^{40}Ar/^{39}Ar$ age (396 ± 3 Ma) may date the peak of earlier regional metamorphism. It was argued by Willner *et al.* (2013*b*) that the peak metamorphic conditions which correspond to burial under a metamorphic field gradient of 20–25 °C km^{-1} could be detected: (1) in relatively undeformed rocks; (2) in rocks showing only D_1 folding; and (3) in rocks strongly overprinted by the D_2 sinistral transcurrent shear. Metamorphic conditions are comparable to those present in foreland fold-and-thrust belts elsewhere (e.g. Fielitz & Mansy, 1999) and require moderate tectonic burial during a compressive event. This event probably occurred prior to D_2 transcurrent deformation which occurred shortly after maximum burial (11–14 km). We therefore relate burial mainly to D_1, but recognize that open to tight upright F_1 folding alone is unlikely to have buried the rocks to such depths on a regional scale. More probable is the explanation that F_1 folds were initially more inclined (as they still are in places) and locally accompanied by oblique reverse faults. Both the inclined folds and faults were then subsequently rotated into more steep attitudes during progressive

https://doi.org/10.1017/S0016756814000508

transpressive shear, which culminated in D_2 sinistral transcurrent movements in the steep shear zones. In such a transposition scenario, the latter therefore incorporated rotated segments of formerly reverse faults. The strike of the transpressive deformation follows the NE trends of the volcanic-sedimentary-plutonic belts of the Mira terrane, which were previously separated by Ediacaran – early Cambrian transtensional movements in the area where the Avalonian microplate was situated at that time.

The prominent Devonian transpressive event appears to have been responsible for the final amalgamation of the dispersed slices of the microcontinent after the onset of collision of Avalonia with the Ganderian margin around 421 Ma (e.g. Murphy, van Staal & Keppie, 1999; van Staal, 2007; van Staal *et al.* 2009). The timing of peak regional metamorphism and the transpressive deformation coincides with Neoacadian events in the now-adjacent Meguma terrane to the south. During the Neoacadian orogeny (400–365 Ma), the Meguma terrane was subjected to widespread collisional deformation and voluminous late- and post-deformational plutonism with related localized high-temperature–low-pressure metamorphism (e.g. White & Barr, 2012). The Neoacadian orogeny is interpreted to have been the result of oblique convergent movement of the Meguma terrane relative to composite Laurentia (including Avalonia) and the main mass of Gondwana to the present-day southeast (Fig. 6a, b). Neoacadian movement between composite Laurentia and Meguma was dextral and accommodated by the east-trending Cobequid–Chedabucto fault zone in mainland Nova Scotia (e.g. Murphy *et al.* 2011). Hence the part of the Meguma terrane now juxtaposed against the Mira terrane was situated farther to the east at the onset of the Neoacadian orogeny, particularly since dextral horizontal translations continued well into the Carboniferous (Murphy *et al.* 2011). However, Meguma is a large terrane that extends SW offshore to southern New England (e.g. Pe-Piper & Loncarevic, 1989; Keen, MacLean & Kay, 1991; Pe-Piper & Jansa, 1999); the piece of Meguma that initially collided with composite Laurentia may therefore now be situated offshore somewhere between Nova Scotia and southern New England. The Neoacadian sinistral motion in the Mira terrane that is coeval with dextral translation along the east–west-oriented Cobequid–Chedabucto Fault Zone appears to form part of a conjugate fault set, which accommodated escape of the Mira terrane towards the NE following convergence with Meguma (Fig. 6a). The wide ductile D_2 shear zones in the Mira terrane developed into more discrete faults in the Carboniferous during exhumation to the surface.

At the time of maximum burial of the Mira terrane, coarse clastic sediments of the McAdams Lake Formation (White & Barr, 1998) were deposited in a half-graben at the boundary between the NW Mira terrane and the adjacent Bras d'Or terrane during the latest Emsian – early Eifelian (*c.* 393 Ma; Cohen, Finney & Gibbard, 2013). Sedimentation occurred in a lacustrine environment during a supposed increase in topographic relief (White & Barr, 1998). Subsequently, clastic sediments of the mainly Tournaisian Horton Group (Martel & Gibling, 1995) were unconformably deposited on the area. Considering an age of the unconformity at the end of the Devonian (*c.* 359 Ma; Cohen, Finney & Gibbard, 2013), time-integrated maximum exhumation rates can be deduced for the Mira terrane since the time of maximum burial to 11–14 km depth (calculated on the basis of a mean crustal density of 2.8 g cm^{-3}) at *c.* 396–385 Ma to exhumation at the surface at *c.* 359 Ma, a period of *c.* 37–26 Ma. Based on these data, the time-integrated exhumation rates were *c.* 0.3–0.5 mm a^{-1}, which is consistent with erosion rates in other tectonically active areas of convergent continental margins (Glodny *et al.* 2005; Willner *et al.* 2005). However, the well-constrained ages of 363±14 Ma (sample 10Ca34; $^{40}Ar/^{39}Ar$) and 365±8 Ma (sample 11Ca05; Rb–Sr) in the SE part of the Mira terrane appear to be in conflict with this calculation, suggesting that exhumation was not uniform. In the SE Mira terrane, the Visean Windsor Group (Boehner, Adams & Giles, 2002) unconformably overlies the Neoproterozoic and Cambrian rocks (Fig. 1). This younger unconformity has an approximate age of *c.* 339 Ma, because the St Peters gabbro and basalt dated by Barr, Grammatikopoulos & Dunning (1994) formed below the base of the Windsor Group. We can therefore derive similar exhumation rates of 0.4–0.6 mm a^{-1}, still consistent with erosion-driven unroofing. In any case, extension-driven unroofing was probably insignificant (if present at all) in the Mira terrane, because brittle-ductile normal faulting has not been recognized in the basement rocks of the Mira terrane and higher exhumation rates exceeding 2 mm a^{-1} would be expected if such a process predominated during exhumation (Thomson, Stoeckhert & Brix, 1998; Ring *et al.* 1999).

6.d. Significance of the transpressive deformation for the assembly of Pangea

The D_2-related transpressive system, which developed during convergence and amalgamation of the Mira and Meguma terranes, is closely related to the closure of the Rheic Ocean, that is the ocean between Laurussia (Laurentia+Baltica+Ganderia+Avalonia+Meguma) and Gondwana (Africa+Armorican terranes). Although strongly overprinted by post-collisional deformation, the approximate location of the Rheic suture has become more apparent in the last decade (e.g. Díez Fernández *et al.* 2011, 2013; van Staal & Barr, 2012; Kroner & Romer 2013; Fig. 6b). Optimal separation is best done using detrital zircon age spectra: Palaeoproterozoic–Mesoproterozoic ages at 1.0–1.8 Ga are prominent in detrital zircon age spectra of the Meguma terrane (Murphy *et al.* 2004; Waldron *et al.* 2009), as is also typical for Ganderian, Avalonian and Amazonian detrital zircon (e.g. Willner *et al.* 2013*a*). In contrast, detrital zircon spectra from West Africa (Abati *et al.* 2012) and the Armorican terranes

https://doi.org/10.1017/S0016756814000508

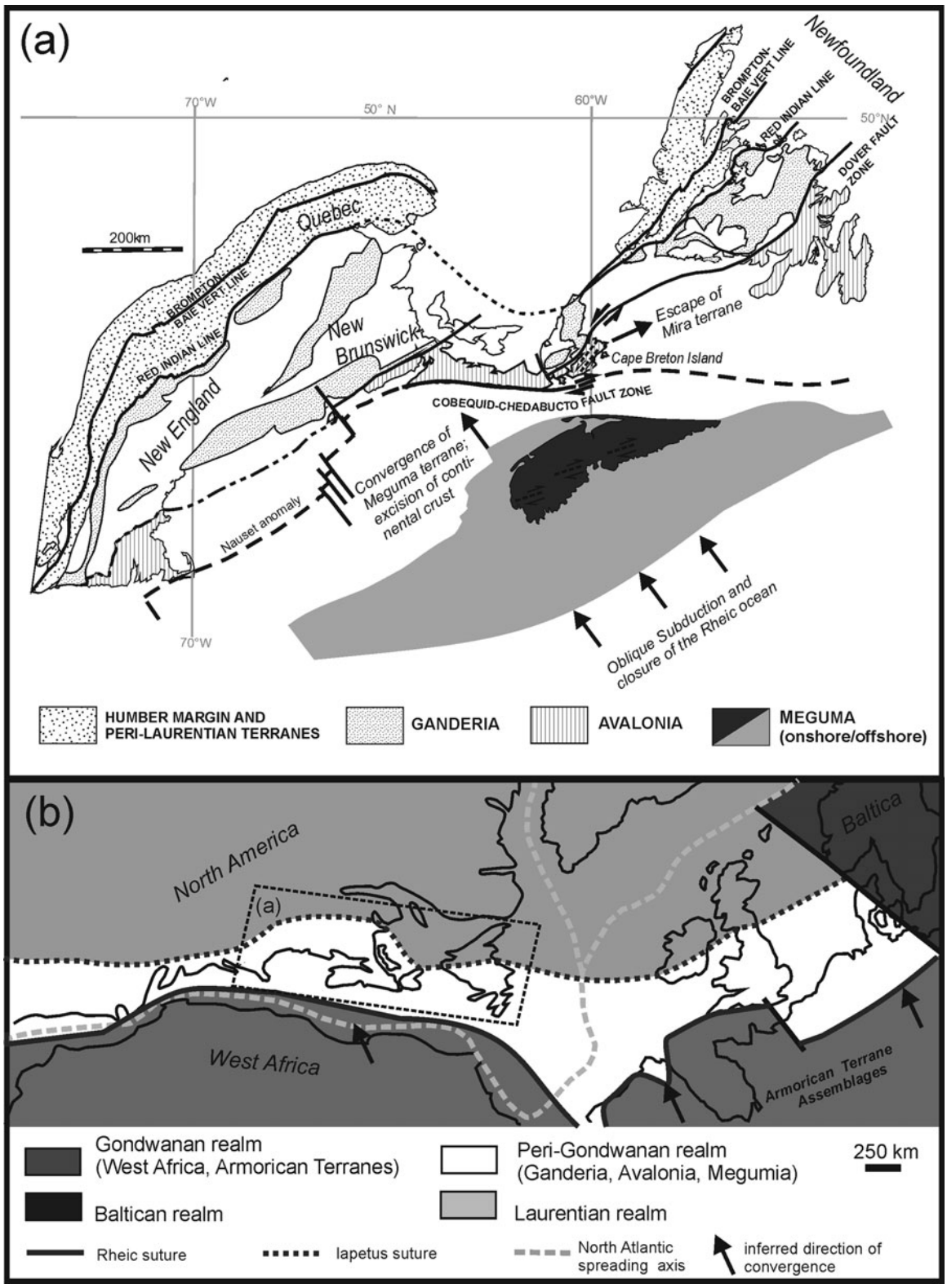

Figure 6. (a) Scenario showing the oblique post-collisional emplacement of the Meguma terrane during the early stages of the Neoacadian orogeny followed by escape of the Mira terrane toward the NE. White areas onshore are mainly Silurian–Carboniferous rock units. (b) Pangean reconstruction showing the approximate locations of the main Iapetus and Rheic sutures.

(Díez Fernández *et al.* 2011) show a gap in this age range. The suture of the Rheic Ocean is therefore likely outboard of what is exposed on land in Atlantic Canada. The nearest known exposure of the suture is within an allochthonous nappe pile in NW Spain on the conjugate margin opposite Newfoundland (Díez Fernández *et al.* 2011, 2013; Fig. 6b). In that area, inferred Rheic oceanic crust is sandwiched between Armorican crust in the bottom and allochthonous crust with inferred North American provenance in the upper

https://doi.org/10.1017/S0016756814000508

part. The closure of the Rheic Ocean, or part of it in NW Spain, at *c.* 380–370 Ma may have been marked by the arrival of Armorican crust in the subduction-exhumation channel beneath relics of Rheic oceanic crust accreted prior to Laurussia (Díez Fernández *et al.* 2011, 2013). This also coincided with the onset of continent–continent collision between Laurussia and Gondwana in Central Europe (Massonne, 2005; Zeh & Gerdes, 2010; Kroner & Romer, 2013). However, the collisional event might have started in this region soon after 400 Ma (e.g. Massonne & O'Brien, 2003; Kroner & Romer, 2013) as evidenced by the tectonic emplacement of mid-ocean-ridge basalt (MORB) -derived eclogites (e.g. Stosch & Lugmair, 1990) in Armorican crustal rocks. These eclogites, which occur in diverse crystalline complexes of the Bohemian Massif, presumably represent subducted fragments of the Rheic Ocean which yielded metamorphic ages in the range 380–400 Ma (e.g. von Quadt & Gebauer, 1993; Beard *et al.* 1995). A model for the plate geometry and geographic constellation of Laurussia and Gondwana, which might have been responsible for the aforementioned ages and tectonics also involving the Mira and Meguma terranes, was proposed by Massonne (2005). In this model, the Rheic Ocean was first completely subducted in the range of central Europe. The continuing movement of Laurussia to the south resulted in the contemporaneous further disappearance of this ocean towards the west and was accompanied by major compressional shear zones trending WSW–ENE.

The NW-directed convergence of Gondwana with Laurussia matches the above inferred direction of convergence between the Meguma and Mira terranes, although during Devonian time the Meguma terrane was located far offshore from its current position relative to the Mira terrane (Fig. 6a). Whether or not oceanic crust existed in the seaway that separated Meguma and Avalonia is not known (e.g. Murphy *et al*. 2004; Waldron *et al*. 2009, 2011), as is the timing of closure of the Rheic Ocean to the SE of Meguma (van Staal & Barr, 2012). However, towards the SW the Rheic Ocean remained open in the Southern Appalachians until the late Carboniferous Alleghanian orogeny. During that time the kinematic pattern of deformation established during the Devonian period remained in Atlantic Canada as in Armorica due to continuing indentation of Gondwana into Laurussia, when deformation became mainly brittle (Murphy & Collins, 2008). With these movements the final assembly of Pangea was completed (Fig. 6b).

6.e. Burial and exhumation of the Mira terrane prior to early Atlantic rifting

The fission track (FT) ages obtained in this study from zircon are in the range of 225 ± 21 Ma to 242 ± 18 Ma, except for a younger age of 151 ± 19 Ma from one locality. Because the closure temperature of this system (circa 250–280 °C; see Section 1) is close to the peak temperature of metamorphism in the Mira terrane, it is expected that ages would be close to the $^{40}Ar/^{39}Ar$ and Rb–Sr ages. However, the zircon FT ages are even younger than the Carboniferous sedimentary cover in the Mira terrane. The data indicate that the metamorphic basement was reburied by sediments and reheated to very low-grade conditions during post-Visean time, followed by re-exhumation and/or cooling during Middle Triassic time. These events took place without affecting either the $^{40}Ar/^{39}Ar$ or Rb–Sr ages. Reheating must therefore have occurred under fluid-absent conditions, as water is essential for element transport, crystallization and recrystallization of mineral phases as well as for isotopic redistribution.

Zircon FT ages were reported previously from the late Palaeozoic rocks in the Minas Basin area in SW Nova Scotia (Ravenhurst *et al.* 1989). Here, the Famennian–Tournaisian–Visean succession (Horton and Windsor groups) including clastic, carbonate and evaporitic rocks was affected by basinal brines at *c.* 330–300 Ma and 250 Ma (K/Ar ages of secondary illite). Zircon in rocks associated with this sequence yielded FT ages similar in part to those in the Mira terrane, but with a wider range from 342 ± 33 Ma to 217 ± 16 Ma (Ravenhurst *et al.* 1989). The zircon FT ages were interpreted as being related to the influx of hot hydrothermal brines. However, this explanation is unlikely in the Mira terrane, where no evidence of post-Devonian hydrothermal activity has been detected. The $^{40}Ar/^{39}Ar$ ages would also have been strongly affected.

Apatite fission track ages in the range of 219–154 Ma were determined in southern Nova Scotia by Ravenhurst *et al.* (1990) and in the range of 247–181 Ma in granitoid rocks and Permian–Triassic sandstone throughout Atlantic Canada by Grist & Zentilli (2003). These apatite FT ages are very similar to our zircon FT ages. Ravenhurst *et al.* (1990) estimated that areas of the present Atlantic margin of Canada were buried under *c.* 4–5 km of strata in upper Palaeozoic intracontinental basins of Pangea and that erosion following basin inversion had removed much of this cover by Late Triassic – Jurassic time. This estimation should be regarded as maximum burial, because the Atlantic margin occurs at the thinned flanks of the Permian–Carboniferous Maritimes Basin with maximum thickness of *c.* 12 km in the depocentre (Sandford & Grant, 1990). Similar burial during Permian time and exhumation prior to Late Triassic – Jurassic rifting associated with the opening of the Central Atlantic Ocean was also proposed for the offshore Maritimes Basin by Ryan & Zentilli (1993), and was shown to be a phenomenon occurring on both sides of the Atlantic.

The high closure temperature of *c.* 250–280 °C for FT in zircon could only be substantially lowered in zircon with high accumulated radiation damage (Rahn *et al.* 2004). However, there is little evidence for this effect in the present samples. Because the thickness of the Permian–Carboniferous cover on the Neoproterozoic rocks was only up to 4–5 km, an increased geothermal gradient of 50–60 °C km^{-1} likely prevailed

https://doi.org/10.1017/S0016756814000508

under these cover sediments, which is typical for rift settings. Evidence for these rift processes includes emplacement of mafic dykes in southern Nova Scotia at 230–220 Ma and 203–185 Ma (Ravenhurst *et al.* 1990; Dunn *et al.* 1998). Heating during this period might have been enhanced within the Mira terrane basement rocks, whereby the lower thermal conductivity of the cover sediments (relative to underlying basement rocks) resulted in a much higher geothermal gradient for the given high heat flow under this 'thermal blanket'. The Central Atlantic Ocean started to open as a westerly extension of the Neotethys (Labails *et al.* 2010; Stampfli & Borel, 2002) at *c.* 190 Ma. At that time the sedimentary cover had largely been eroded and the basement rocks had cooled to temperatures below the closure temperature of the apatite fission track system (Ravenhurst *et al*. 1990; Ryan & Zentilli, 1993; Grist & Zentilli, 2003).

7. Conclusions

Using a multi-method dating approach in very low- to low-grade metamorphic rocks we have derived more details of the timing of tectonometamorphic geological processes in the Mira terrane including influx of hydrous fluids, metamorphism, deformation, burial and exhumation.

An age signal related to a penetrative hydrothermal overprint at *c.* 560–510 Ma as indicated by a regional pervasive $\delta^{18}O$ depletion (Potter, Longstaffe & Barr, 2008; Potter *et al.* 2008) was not detected in the samples dated during the present study. White mica, if formed at this stage, must have been completely recrystallized in those samples due to breakdown and production of internally generated metamorphic fluids, which would not have altered the oxygen isotope signature.

Sparse relict $^{40}Ar/^{39}Ar$ spot age clusters of 465–477 Ma and *c.* 439 Ma could be related to meteoric fluid influx during extensional events. Spot ages of *c.* 420–428 Ma could be related to early burial during Acadian collision of Avalonia with the composite Laurussia margin. However, incomplete resetting of older ages cannot be excluded with the present dataset. Evidently, the Mira terrane was situated in the foreland of the Acadian collision and escaped pervasive Acadian tectonometamorphic overprinting. Only $^{40}Ar/^{39}Ar$ analysis of single spots by laser ablation enables detection of age heterogeneity at thin-section scale at very low- to low-grade metamorphism.

Most $^{40}Ar/^{39}Ar$ and Rb–Sr ages of white mica fall within the range 396–366 Ma. The oldest age may reflect mineral growth at peak very low- to low-grade metamorphic conditions during a main pulse of influx of internally generated metamorphic fluids, but the bulk of the ages are interpreted to be related to shearing during sinistral transpressive deformation. This deformation was concomitant with dextral transpression of the Meguma terrane with composite Laurentia (including Avalonia), which locally resulted in a conjugate fault set such that Mira and other parts of Avalonia escaped to the NE (Neoacadian event). Exhumation from maximum burial to the surface began at *c.* 390 Ma in the NW part of the Mira terrane and ended in the SW at *c.* 340 Ma. Exhumation rates of 0.3–0.6 mm a^{-1} indicate erosion-driven unroofing. During exhumation, transpressive ductile shear zones became more discrete resulting in a prominent Carboniferous conjugate fault set. Intrusion of A- and I-type granitoids also occurred during this time period. The Neoacadian transpressive event is related to the closure of the Rheic Ocean along a suture outside Atlantic Canada, where Gondwana and Laurussia converged to form the supercontinent of Pangea. The importance of Neoacadian events in Atlantic Canada for the closure of the Rheic Ocean is highlighted here for the first time.

Zircon fission track ages of 225–242 Ma indicate post-collisonal late Palaeozoic reburial of the Mira terrane rocks within intracontinental basins of Pangea under fluid-absent conditions, and date cooling to temperatures <250 °C related to elevated geothermal gradients and exhumation during Late Triassic rift events prior to opening of the Central Atlantic Ocean.

Supplementary material

To view supplementary material for this article, please visit http://dx.doi.org/10.1017/S0016756814000508

Acknowledgements. This project was financed by Deutsche Forschungsgemeinschaft (grants Ma1126-27-1,2 and Wi847-9-1,2) to HJM and APW. Geological mapping by SMB and CEW in SE Cape Breton Island was funded by the Geological Survey of Canada through the 1984–1989 Canada – Nova Scotia Mineral Development Agreement and the 1990–1992 Canada – Nova Scotia Cooperation Agreement, as well as by research grants to SMB from the Natural Sciences and Engineering Research Council of Canada. Valuable comments by editor M. Allen and an anonymous reviewer improved the manuscript.

References

ABATI, J., AGHZER, A.M., GERDES, A. & ENNIH, N. 2012. Insights on the crustal evolution of the West African Craton from Hf isotopes in detrital zircons from the Anti-Atlas belt. *Precambrian Research* **183**, 263–74.

BARR, S. M. 1993. Geochemistry and tectonic setting of late Precambrian volcanic and plutonic rocks in southeastern Cape Breton Island, Nova Scotia. *Canadian Journal of Earth Science* **30**, 1147–54.

BARR, S. M., DUNNING, G. R., RAESIDE, R. P. & JAMIESON, R. A. 1990. Contrasting U-Pb ages from plutons in the Bras d'Or and Mira terranes of Cape Breton Island, Nova Scotia. *Canadian Journal of Earth Science* **27**, 1200–8.

BARR, S. M., GRAMMATIKOPOULOS, A. L. & DUNNING, G. R. 1994. Early Carboniferous gabbro and basalt in the St. Peters area, southern Cape Breton Island, Nova Scotia. *Atlantic Geology* **30**, 247–58.

BARR, S. M. & MACDONALD, A. S. 1992. Devonian plutons in southeastern Cape Breton Island, Nova Scotia. *Atlantic Geology* **28**, 101–13.

BARR, S. M. & RAESIDE, R. P. 1989. Tectonostratigraphic terranes in Cape Breton Island, Nova Scotia.

Implications for the configuration of the northern Appalachian Orogen. *Geology* **17**, 822–5.

BARR, S. M., WHITE, C. E., HAMES, W. E. & REYNOLDS, P. H. 2014. Age and provenance of detrital muscovite from the Ediacaran-Cambrian boundary zone in Atlantic Canada: Implications for the paleogeographic position of Avalonia. *GAC-MAC Conference Fredericton, Program with Abstracts* **37**, 18–19.

BARR, S. M., WHITE, C. E. & MACDONALD, A. S. 1996. Stratigraphy, tectonic setting, and geologic history of Late Precambrian volcanic-sedimentary-plutonic belts in southeastern Cape Breton Island, Nova Scotia. *Geological Survey of Canada Bulletin* **468**, 84 pp.

BEARD, B. L., MEDARIS, L. G., JR., JOHNSON, C. M., JELINEK, E., TONIKA, J. & RICIPUTI, L. R. 1995. Geochronology and geochemistry of eclogites from the Mariánské Lázně Complex, Czech Republic: Implications for Variscan orogenesis. *Geologische Rundschau* **84**, 552–67.

BEVIER, M. L., BARR, S. M., WHITE, C. E. & MACDONALD, A. S. 1993. U-Pb geochronologic constraints on the volcanic evolution of the Mira (Avalon) terrane, southeastern Cape Breton Island, Nova Scotia. *Canadian Journal of Earth Science* **30**, 1–10.

BOEHNER, R. C., ADAMS, G. C. & GILES, P. S. 2002. Karst geology in the salt-bearing Windsor Group evaporites and controls on the origin of gypsum deposits in south-central Cape Breton Island, Nova Scotia. Mineral Resources Branch, Nova Scotia Department of Natural Resources, Report of Activities 2003–1, 9–24.

BRIX, M. R., STÖCKHERT, B., SEIDEL, E., THEYE, T., THOMSON, S. N. & KÜSTER, M. 2002. Thermobarometric data from a fossil zircon partial annealing zone in high pressure-low temperature rocks of eastern and central Crete, Greece. *Tectonophysics* **349**, 309–26.

COHEN, K. M., FINNEY, S. & GIBBARD, P. L. 2013. International Chronostratigraphic Chart, Version 01/2013. International Commision on Stratigraphy.

DÍEZ FERNÁNDEZ, R., FOSTER, D. A., GÓMEZ BARREIRO, J. & ALONSO-GARCÍA, M. 2013. Rheological control on the tectonic evolution of a continental suture zone: the Variscan example from NW Iberia (Spain). *International Journal of Earth Science* **102**, 1305–19.

DÍEZ FERNÁNDEZ, R., MARTÍNEZ CATALÁN, J. R., ARENAS, R. & ABATI, J. 2011. Tectonic evolution of a continental subduction-exhumation channel: Variscan structure of the basal allochthonous units in NW Spain. *Tectonics* **30**, TC3009, 3001–22.

DUNN, A. M., REYNOLDS, P. H., CLARKE, D. B. & UGIDOS, J. M. 1998. A comparison of the age and composition of the Shelburne dyke, Nova Scotia, and the Messejana dyke, Spain. *Canadian Journal of Earth Sciences* **35**, 1110–5.

FIELITZ, W. & MANSY, J.-L. 1999. Pre- and synorogenic burial metamorphism in the Ardennes and neighbouring areas (Rhenohercynian zone, central European Variscides). *Tectonophysics* **309**, 227–56.

FREEMAN, S. R., BUTLER, R. W. H., CLIFF, R. A. & REX, D. C. 1998. Direct dating of mylonite evolution: a multidisciplinary geochronological study from the Moine Thrust Zone, NW Scotland. *Journal of the Geological Society, London* **155**, 745–58.

GALBRAITH, R. F. & LASLETT, G. M. 1993. Statistical models for mixed fission track ages. *Nuclear Tracks and Radiation Measurements* **21**, 459–70.

GIBLING, M. R., CULSHAW, N., RYGEL, M. C. & PASCUCCI, V. 2008. The Maritimes basin of Atlantic Canada: basin creation and destruction in the collisional zone of Pangea. *Sedimentary Basins of the World* **5**, 211–44.

GILES, P. S., NAYLOR, R. D., TENIERE, P. J., WHITE, C. E., BARR, S. M., DEMONT, G. J. & FORCE, E. R. 2010. Bedrock geology map of the Port Hawkesbury area, Part of NTS Sheets 11F/06, 11F/07, 11F/10, 11F/11 and 11F/15, Inverness, Richmond, Guysborough, and Antigonish Counties, Nova Scotia (scale 1:50 000). Nova Scotia Department of Natural Resources, Mineral Resources Branch, Open File Map Me 2010–006.

GLODNY, J., LOHRMANN, J., ECHTLER, H., GRÄFE, K., SEIFERT, W., COLLAO, S. & FIGUEROA, O. 2005. Internal dynamics of a paleoaccretionary wedge: insights from combined isotope tectonochronology and sandbox modelling of the South–Central Chilean forearc. *Earth and Planetary Science Letters* **231**, 23–39.

GLODNY, J., RING, U. & KÜHN, A. 2008. Coeval high-pressure metamorphism, thrusting, strike-slip, and extensional shearing in the Tauern Window, Eastern Alps. *Tectonics* **27**, TC4004.

GREEN, P. F., DUDDY, I. R., LASLETT, G. M., HEGARTY, K. A., GLEADOW, A. J. W. & LOVERING, J. F. 1989. Thermal annealing of fission tracks in apatite, 4. Quantitative modelling techniques and extension to geological timescales. *Chemical Geology* **79**, 155–82.

GRIST, A. M. & ZENTILLI, M. 2003. Post-Paleocene cooling in the southern Canadian Atlantic region: evidence from apatite fission track models. *Canadian Journal of Earth Science* **40**, 1279–97.

HIBBARD, J. P., VAN STAAL, C. R., RANKIN, D. & WILLIAMS, H. 2006. Lithotectonic map of the Appalachian orogen (north), Canada–United States of America. Geological Survey of Canada Map 2041A, scale 1:1,500,000.

HURFORD, A. J. 1990. Standardization of fission-track dating calibration: recommended by the Fission-track Working Group of the IUGS Subcommission on Geochronology. *Chemical Geology (Isotope Geoscience Section)* **80**, 171–8.

HURFORD, A. J. & GREEN, P. F. 1983. The zeta age calibration of fission-track dating. *Isotope Geoscience* **1**, 285–317.

HUTCHINSON, R. D. 1952. *The Stratigraphy and Trilobite Faunas of the Cambrian Sedimentary Rocks of Cape Breton Island, Nova Scotia*. Geological Survey of Canada, Memoir no. 263, 124 pp.

INGER, S. & CLIFF, R. A. 1994. Timing of metamorphism in the Tauern Window, Eastern Alps: Rb-Sr ages and fabric formation. *Journal of Metamorphic Geology* **12**, 695–707.

ISHIZUKA, O., YUASA, M. & UTO, K. 2002. Evidence of porphyry copper-type hydrothermal activity from a submerged remnant back-arc volcano of the Izu-Bonin arc: implication for the volcanotectonic history of backarc seamounts. *Earth and Planetary Science Letters* **198**, 381–99.

KEEN, C. E., MACLEAN, B. C. & KAY, W. A. 1991. A deep seismic reflection profile across the Nova Scotia continental margin, offshore eastern Canada. *Canadian Journal of Earth Sciences* **28**, 1112–20.

KELLEY, S. P., ARNAUD, N. O. & TURNER, S. P. 1994. High spatial resolution 40Ar/39Ar investigations using an ultra-violet laser probe extraction technique. *Geochimica Cosmochimica Acta* **58**, 3519–25.

KRONER, U. & ROMER, R. L. 2013. Two plates - many subduction zones: the Variscan orogeny reconsidered. *Gondwana Research* **24**, 298–329.

LABAILS, C., OLIVET, J. L., ASLANIAN, D. & ROEST, W. R. 2010. An alternative early opening scenario for the

Central Atlantic Ocean. *Earth and Planetary Science Letters* **297**, 355–68.

LANDING, E. 1991. Upper Precambrian through Lower Cambrian of Cape Breton Island: faunas, paleoenvironments, and stratigraphic revision. *Journal of Paleontology* **65**, 570–95.

LUDWIG, K. 2009. *Isoplot v. 3.71: A Geochronological Toolkit for Microsoft Excel*. Berkeley Geochronology Center, Berkeley, California, Special Publication **4**, 70 pp.

MACDONALD, A. S. & BARR, S. M. 1993*a*. Geological setting and depositional environment of the Stirling Group of southeastern Cape Breton Island, Nova Scotia. *Atlantic Geology* **29**, 137–47.

MACDONALD, A. S. & BARR, S. M. 1993*b*. The Blue Mountain polymetallic skarn and associated porphyry dykes, southeastern Cape Breton Island, Nova Scotia. In *Mineral Deposit Studies in Nova Scotia II* (ed. A. L. Sangster), pp. 3–18. Geological Survey of Canada, Paper 91–9.

MARTEL, A. T. & GIBLING, M. R. 1995. Stratigraphy and tectonic history of the Upper Devonian to Lower Carboniferous Horton Bluff Formation, Nova Scotia. *Atlantic Geology* **32**, 13–38.

MASSONNE, H.-J. 2005. Involvement of crustal material in delamination of the lithosphere after continent-continent collision. *International Geology Review* **47**, 792–804.

MASSONNE, H.-J. & O'BRIEN, P. J. 2003. The Bohemian Massif and the NW Himalaya. In *Ultrahigh Pressure Metamorphism* (eds D. A. Carswell & R. Compagnoni), pp. 145–87. EMU Notes in Mineralogy no. 5.

MASSONNE, H.-J. & WILLNER, A. P. 2008. Phase relations and dehydration behaviour of psammopelite and mid-ocean ridge basalt at very low-grade to low-grade metamorphic conditions. *European Journal of Mineralogy* **20**, 867–79.

MCDOUGALL, I. & HARRISON, T. M. 1999. *Geochronology and Thermochronology by the $^{40}Ar/^{39}Ar$ Method*. Oxford: Oxford University Press, 269 pp.

MCMULLIN, D. W. A., BARR, S. M. & RAESIDE, R. P. 2010. Very low- and low-grade metamorphism of mafic volcanic rocks of the Mira terrane (Avalonia), southeastern Cape Breton Island, Nova Scotia. *Atlantic Geology* **46**, 95–126.

MÜLLER, W., DALLMEYER, R. D., NEUBAUER, F. & THÖNI, M. 1999. Deformation-induced resetting of Rb/Sr and $^{40}Ar/^{39}Ar$ mineral systems in a low-grade, polymetamorphic terrane (Eastern Alps Austria). *Journal of the Geological Society, London* **156**, 261–78.

MURPHY, J. B. & COLLINS, A. S. 2008. ^{40}Ar–^{39}Ar white mica ages reveal Neoproterozoic/Paleozoic provenance and an Alleghanian overprint in coeval Upper Ordovician–Lower Devonian rocks of Meguma and Avalonia. *Tectonophysics* **461**, 265–76.

MURPHY, J. B., FERNANDEZ-SUAREZ, J., KEPPIE, J. D. & JEFFRIES, T. E. 2004. Contiguous rather than discrete Paleozoic histories for the Avalon and Meguma Terranes based on detrital zircon data. *Geology* **32**, 585–8.

MURPHY, J. B., VAN STAAL, C. R. & KEPPIE, J. D. 1999. Middle to late Paleozoic Acadian orogeny in the northern Appalachians: A Laramide-style plume-modified orogeny? *Geology* **27**, 653–6.

MURPHY, J. B., WALDRON, J. W. F., KONTAK, D. J., PE-PIPER, G. & PIPER, D. J. W. 2011. Minas Fault Zone: Late Paleozoic history of an intra-continental orogenic transform fault in the Canadian Appalachians. *Journal of Structural Geology* **33**, 312–28.

PALACIOS, T., JENSEN, S., BARR, S. M. & WHITE, C. E. 2009. Acritarchs from the MacLean Brook Formation, southeastern Cape Breton Island, Nova Scotia: new data on middle Cambrian-Furongian acritarch zonation. *Palaeogeography, Palaeoclimatology, Palaeoecology* **273**,123–41.

PE-PIPER, G. & JANSA, L. F. 1999. Pre-Mesozoic basement rocks offshore Nova Scotia, Canada: New constraints on the accretion history of the Meguma terrane. *Geological Society of America Bulletin* **111**, 1773–91.

PE-PIPER, G. & LONCAREVIC, B. D. 1989. Offshore continuation of Meguma terrane, southwestern Nova Scotia. *Canadian Journal of Earth Sciences* **26**, 176–91.

POTTER, J., LONGSTAFFE, F. J. & BARR, S. M. 2008. Regional 18O-depletion of Neoproterozoic igneous rocks from Avalonia, Cape Breton Island and southern New Brunswick, Canada. *Geological Society of America Bulletin* **120**, 347–67.

POTTER, J., LONGSTAFFE, F. J., BARR, S. M., THOMPSON, M. D. & WHITE, C. E. 2008. Altering Avalonia: oxygen isotopes and terrane distinction in the Appalachian peri-Gondwanan realm. *Canadian Journal of Earth Science* **45**, 815–25.

RAESIDE, S. M. & BARR, S. M. 1990. Geology and tectonic development of the Bras d'Or suspect terrane, Cape Breton Island, Nova Scotia. *Canadian Journal of Earth Sciences* **27**, 1371–81.

RAHN, M. K., BRANDON, M. T., BATT, G. E. & GARVER, J. I. 2004. A zero-damage model for fission-track annealing in zircon. *American Mineralogist* **89**, 473–84.

RAVENHURST, C. E., DONELICK, R., ZENTILLI, M., REYNOLDS, P. H. & BEAUMONT, C. 1990. A fission track pilot study of thermal effects of rifting on the onshore Nova Scotian margin, Canada. *Nuclear Tracks Radiation Measurements* **17**, 373–8.

RAVENHURST, C. E., REYNOLDS, P. H., ZENTILLI, M., KRUEGER, H. W. & BLENKINSOP, J. 1989. Formation of Carboniferous Pb-Zn and barite mineralization from basin-derived fluids, Nova Scotia, Canada. *Economic Geology* **84**, 1471–88.

REYNOLDS, P. H., BARR, S. M. & WHITE, C. E. 2009. Provenance of detrital muscovite in Cambrian Avalonia of Maritime Canada: $^{40}Ar/^{39}Ar$ ages and chemical compositions. *Canadian Journal of Earth Sciences* **46**, 169–80.

RING, U., BRANDON, M. T., WILLETT, S. D. & LISTER, G. S. 1999. Exhumation processes. In *Exhumation Processes: Normal Faulting, Ductile Flow and Erosion* (eds U. Ring, M. T. Brandon, G. S. Lister & S. D. Willett), pp. 1–27. Geological Society of London, Special Publication no. 154.

RYAN, R. J. & ZENTILLI, M. 1993. Allocyclic and thermochronological constraints on the evolution of the Maritimes Basin of eastern Canada. *Atlantic Geology* **29**, 187–97.

SANFORD, B. V. & GRANT, A. C. 1990. Bedrock geological mapping and basin studies in the Gulf of St. Lawrence. Current research, part B. *Geological Survey of Canada, Paper* **90–1B**, 33–42.

STAMPFLI, G. M. & BOREL, G. D. 2002. A plate tectonic model for the Paleozoic and Mesozoic constrained by dynamic plate boundaries and restored synthetic oceanic isochrons. *Earth and Planetary Science Letters* **196**, 17–33.

STEIGER, R. H. & JÄGER, E. 1977. Subcommission on geochronology: convention on the use of decay constants in geo- and cosmochronology. *Earth and Planetary Science Letters* **36**, 359–62.

STOSCH, H.-G. & LUGMAIR, G. W. 1990. Geochemistry and evolution of MORB-type eclogites from the Münchberg Massif, southern Germany. *Earth and Planetary Science Letters* **99**, 230–49.

TAGAMI, T., GALBRAITH, R. F., YAMADA, R. & LASLETT, G. M. 1998. Revised annealing kinetics of fission tracks in zircon and geological implications. In *Advances in Fission-Track Geochronology* (eds P. Van den Haute & F. De Corte), pp. 99–112. Dordrecht: Kluwer Academic Publishers.

THOMSON, S. N. & RING, U. 2006. Thermochronologic evaluation of postcollision extension in the Anatolide Orogen, western Turkey. *Tectonics* **25**, TC3005, doi: 10.1029/2005TC001833.

THOMSON, S. N., STOECKHERT, B. & BRIX, M. R. 1998. Thermochronology of the high-pressure metamorphic rocks of Crete, Greece: implications for the speed of tectonic processes. *Geology* **26**, 259–62.

UTO, K., ISHIZUKA, O., MATSUMOTO, A., KAMIOKA, H. & TOGASHI, S. 1997. Laser-heating 40Ar/39Ar dating system of the Geological Survey of Japan: system outlines and preliminary results. *Bulletin of the Geological Survey of Japan* **48**, 23–46.

VAN STAAL, C. R. 2007. Pre-Carboniferous tectonic evolution and metallogeny of the Canadian Appalachians. In *Mineral Deposits of Canada: A Synthesis of Major Deposit-Types, District Metallogeny, the Evolution of Geological Provinces, and Exploration Methods* (ed. W. D. Goodfellow), pp. 793–818. Geological Association of Canada, Mineral Deposits Division, Special Publication no. 5.

VAN STAAL, C. R. & BARR, S. M. 2012. Lithospheric architecture and tectonic evolution of the Canadian Appalachians and associated Atlantic margin. Chapter 2 In *Tectonic Styles in Canada: the LITHOPROBE Perspective* (eds J. A. Percival, F. A. Cook & Clowes), pp. 41–95. Geological Association of Canada, Special Paper no. 49.

VAN STAAL, C. R., WHALEN, J. B., VALVERDE-VAQUERO, P., ZAGOREVSKI, A. & ROGERS, N. 2009. Pre-Carboniferous, episodic accretion-related, orogenesis along the Laurentian margin of the northern Appalachians. In *Ancient Orogens and Modern Analogues* (eds J. B. Murphy, J. D. Keppie & A. J. Hynes), pp. 271–316. Geological Society London, Special Publication no. 327.

VERMEESCH, P. 2009. RadialPlotter: a Java application for fission track, luminescence and other radial plots. *Radiation Measurements* **44**, 409–10.

VILLA, I. M. 1998. Isotopic closure. *Terra Nova* **10**, 42–7.

VILLA, I. M. 2006. From nanometer to megameter: Isotopes, atomic-scale processes, and continent-scale tectonic models. *Lithos* **87**, 155–73.

VON QUADT, A. & GEBAUER, D. 1993. Sm-Nd and U-Pb dating of eclogites and granulites from the Oberpfalz, NE Bavaria, Germany. *Chemical Geology* **109**, 317–39.

WALDRON, J. W. F., SCHOFIELD, D. I., WHITE, C. E. & BARR, S. M. 2011. Cambrian successions of the Meguma Terrane, Nova Scotia, Canada, and Harlech Dome, North Wales, UK: dispersed fragments of a peri-Gondwanan basin? *Journal of the Geological Society, London* **168**, 83–98.

WALDRON, J. W. F., WHITE, C. E., BARR, S. M., SIMONETTI, A. & HEAMAN, L. M. 2009. Provenance of the Meguma terrane, Nova Scotia: rifted margin of early Paleozoic Gondwana. *Canadian Journal of Earth Sciences* **46**, 1–8.

WHITE, C. E. & BARR, S. M. 1998. Stratigraphy and tectonic significance of the Lower to Middle Devonian McAdams Lake Formation, Cape Breton Island, Nova Scotia. *Atlantic Geology* **34**, 133–45.

WHITE, C. E. & BARR, S. M. 2012. The new Meguma: stratigraphy, metamorphism, paleontology and provenance. *Field Trip B-5*, Geological Association of Canada and Mineralogical Association of Canada, 68 pp.

WHITE, C. E., BARR, S. M. & KETCHUM, J. W. F. 2003. New age controls on rock units in pre-Carboniferous basement blocks in southwestern Cape Breton Island and adjacent mainland Nova Scotia. Nova Scotia Department of Natural Resources, Minerals and Energy Branch, Report of Activities 2002, Report ME 2003–1, 163–78.

WHITE, C. E., BARR, S. M., REYNOLDS, P. H., GRACE, E. & MCMULLIN, D. W. A. 2006. The Pocologan Metamorphic Suite: High-pressure metamorphism in a Silurian fore-arc complex, Kingston Terrane, southern New Brunswick. *Canadian Mineralogist* **44**, 905–27.

WIJBRANS, J. R. & MCDOUGALL, I. 1986. $^{40}Ar/^{39}Ar$ dating of white micas from an Alpine high-pressure belt on Naxos (Greece): resetting of the argon isotopic system. *Contributions to Mineralogy and Petrology* **93**, 187–94.

WILLNER, A. P., GERDES, A., MASSONNE, H.-J., BARR, S. M. & WHITE, C. E. 2013*a*. Origin and crustal evolution of the Avalonian microcontinent: evidence from a U-Pb and Lu-Hf isotope study of detrital zircon in Nova Scotia, Canada, and East Belgium. *Journal of the Geological Society, London* **170**, 769–84.

WILLNER, A. P., MASSONNE, H.-J., BARR, S. M. & WHITE, C. E. 2013*b*. Very low- to low-grade metamorphic processes related to the collisional assembly of Avalonia in SE Cape Breton Island (Nova Scotia, Canada). *Journal of Petrology* **54**, 1849–74.

WILLNER, A. P., MASSONNE, H.-J., RING, U., SUDO, M. & THOMSON, S. N. 2012. P–T evolution and timing of a late Palaeozoic fore-arc system and its heterogeneous Mesozoic overprint in north-central Chile (latitudes 31–32°S).*Geological Magazine* **149**, 177–207.

WILLNER, A. P., SEPÚLVEDA, F. A., HERVÉ, F., MASSONNE, H.-J. & SUDO, M. 2009. Conditions and timing of pumpellyite-actinolite facies metamorphism in the Early Mesozoic frontal accretionary prism of the Madre de Dios Archipelago (50° 20ć S; S-Chile). *Journal of Petrology* **50**, 2127–55.

WILLNER, A. P., THOMSON, S. N., KRÖNER, A., WARTHO, J. A., WIJBRANS, J. & HERVÉ, F. 2005. Time markers for the evolution and exhumation history of a late Palaeozoic paired metamorphic belt in central Chile (34°–35° 30°S). *Journal of Petrology* **46**, 1835–58.

ZEH, A. & GERDES, A. 2010. Baltica- and Gondwana-derived sediments in the Mid-German Crystalline Rise (Central Europe): implications for the closure of the Rheic Ocean. *Gondwana Research* **17**, 254–63.